
PARAMETER-EFFICIENT FINE-TUNING OF STATE SPACE MODELS

Kevin Galim*

FuriosaAI

kevin.galim@furiosa.ai

Wonjun Kang*

FuriosaAI

Seoul National University

Yuchen Zeng*

UW-Madison

yzeng58@wisc.edu

Hyung Il Koo

FuriosaAI

Ajou University

hikoo@furiosa.ai

Kangwook Lee

UW-Madison

kangwook.lee@wisc.edu

* Equal contribution. Authors listed in alphabetical order.

ABSTRACT

Deep State Space Models (SSMs), such as Mamba (Gu & Dao, 2024), have become powerful tools for language modeling, offering high performance and linear scalability with sequence length. However, the application of parameter-efficient fine-tuning (PEFT) methods to SSM-based models remains underexplored. We start by investigating two fundamental questions on existing PEFT methods: (i) How do they perform on SSM-based models? (ii) Which parameters should they target for optimal results? Our analysis shows that LoRA and its variants consistently outperform all other PEFT methods. While LoRA is effective for linear projection matrices, it fails on SSM modules—yet still outperforms other methods applicable to SSMs, indicating their limitations. This underscores the need for a specialized SSM tuning approach. To address this, we propose Sparse Dimension Tuning (SDT), a PEFT method tailored for SSM modules. Combining SDT for SSMs with LoRA for linear projection matrices, we achieve state-of-the-art performance across extensive experiments.

1 Introduction

In the past few years, Large Language Models (LLMs) such as ChatGPT (Achiam et al., 2023; Brown et al., 2020) have achieved groundbreaking performance and are now widely used in daily life. While many models rely on the Transformer architecture (Vaswani et al., 2017), its quadratic time complexity due to the attention mechanism poses challenges for long sequences. To address this, alternative architectures such as Linear Attention (Katharopoulos et al., 2020), RWKV (Peng et al., 2023), RetNet (Sun et al., 2023), and Mamba (Gu & Dao, 2024) have been developed, offering subquadratic time complexity. Efficient attention alternatives often rely on State Space Models (SSMs) or their variants (Gu et al., 2021, 2022b,a; Gu & Dao, 2024), which are akin to linear RNNs, maintaining hidden states for sequential processing. S4 (Gu et al., 2022b,a) overcomes RNNs’ parallel training limitations by constraining parameter structures, enabling a convolutional form for efficient parallel computation. S6 (Gu & Dao, 2024) improves this with input-dependent parameters, enabling selective focus on relevant information per token. Building on S6 with linear projection matrices (analogous to the Feed-Forward Networks in Transformer layers), Mamba-I (Gu & Dao, 2024) emerged as a prominent SSM-based model. It was later extended to Mamba-II (Dao & Gu, 2024), with both models achieving Transformer-level performance in language modeling and gaining widespread recognition.

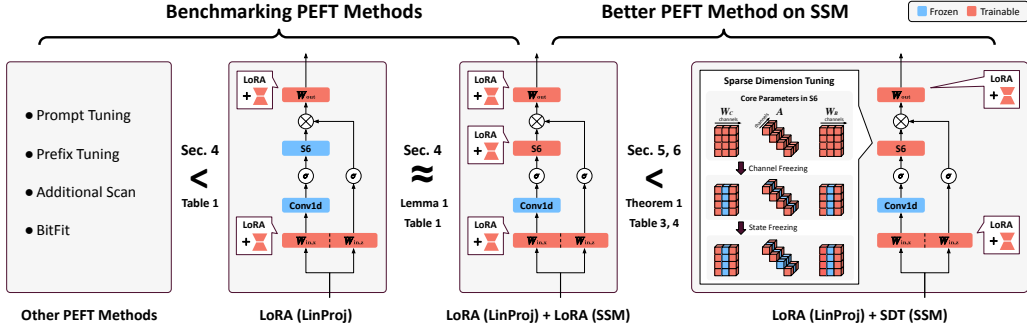


Figure 1: **A visual guide to PEFT methods in SSM-based models: benchmarking and innovation.** We compare various existing PEFT approaches on SSM-based models, demonstrating that LoRA applied to linear projection matrices outperforms all other methods. However, extending LoRA to SSM modules fails to yield further improvements. To address this, we propose Sparse Dimension Tuning (SDT), which achieves state-of-the-art performance on SSM-based models when combined with LoRA for linear projection matrices.

As SSMs gain popularity, performing parameter-efficient fine-tuning (PEFT) on pretrained models for downstream tasks is crucial, since full fine-tuning is costly and inefficient. Numerous PEFT methods (Houlsby et al., 2019; Hu et al., 2021; He et al., 2021; Li & Liang, 2021; Lester et al., 2021; Zaken et al., 2022; Liu et al., 2021, 2022; Houlsby et al., 2019) have been developed, achieving notable success on Transformer models. The most popular PEFT methods fall into three categories: (i) *input-injected methods*, which add sequences to the model’s main input (Lester et al., 2021) or prepend tokens to the intermediate inputs at each layer (Li & Liang, 2021); (ii) *architecture-enhanced methods*, which adjust the model architecture. For example, Houlsby et al. (2019) added layers between Transformer layers, while Additional-scan (Yoshimura et al., 2024) expands state dimensions in the SSM module; (iii) *weight-tuning methods*, which directly modify existing model weights. Notable weight-tuning approaches include BitFit (Zaken et al., 2022), which updates only bias terms, and LoRA (Hu et al., 2021), which modifies weight matrices through low-rank updates, along with its variants such as DoRA (Liu et al., 2024) and LoRA+ (Hayou et al., 2024). For simplicity, we denote LoRA and its variants as LoRA*.

Despite the success that existing PEFT methods have achieved in adapting Transformer-based models, their efficacy in adapting SSM-based models remains largely underexplored, leaving many interesting questions open.

1. *Do existing popular PEFT methods remain effective for SSM-based models?*
2. *If applicable, what is the optimal way to integrate these methods into SSM-based models, and which parameters should be updated?*
3. *If not, can we design specialized variants tailored to SSMs that yield superior performance?*

Our main contributions to address these questions are:

- **Comprehensive Benchmarking of PEFT Methods.** We benchmark six widely used PEFT methods across three categories on diverse tasks, including natural language understanding, generation, and computer vision. We evaluate these methods on both SSM-based models (i.e., Mamba) and a hybrid model (i.e., Jamba (Lieber et al., 2024)), which consists of both Transformer layers and Mamba layers. Our results show that LoRA* consistently outperforms all other PEFT methods on both SSM-based and hybrid models. However, its effectiveness is limited to linear projection matrices, as further tuning of SSM modules does not improve performance. Among methods applicable to SSM modules, LoRA* remains the top performer, underscoring the urgent need for a specialized approach to tuning SSM modules.
- **Introducing Sparse Dimension Tuning (SDT) for SSM Modules.** To develop an effective method for tuning SSM modules, we conduct a theoretical analysis to understand the roles of different parameters. This analysis motivates the *Sparse Dimension Tuning and Pruning* (SDT-P) method, which improves efficiency by freezing and pruning certain channel and state dimensions while training only the remaining ones. We establish theoretical guarantees for its effectiveness in SSM-based models when combined with LoRA applied to linear projection matrices. We then simplify

SDT-P into *Sparse Dimension Tuning* (SDT) by omitting explicit pruning, as pruned dimensions can be considered equivalent to training dimensions set to zero. SDT selectively updates channels and fine-tunes specific dimensions within them, as illustrated in Fig. 1.

- **Demonstrating Effectiveness of SDT.** Through extensive experiments, we demonstrate that integrating SDT into SSM-based models, combined with applying LoRA* to their linear projection matrices, achieves state-of-the-art fine-tuning performance.

The roadmap of our paper is illustrated in Fig. 1. All of our code is available at <https://github.com/furiosa-ai/ssm-peft>.

Scope of the study. We focus on SSM-based models by (i) benchmarking existing PEFT methods and (ii) introducing an effective PEFT method specifically tailored to SSM modules. While we benchmark different parameter configurations unique to each layer (details in Sec. C), our primary aim is to offer a broader comparison across the SSM module and the linear projection matrices rather than delving into highly specific, architecture-dependent parameters (e.g., x_{proj}). Regarding the SSM-specific method, we emphasize that our intention is *not* to propose a novel technique applicable *beyond* SSM; instead, we focus on SSMs exclusively by identifying an effective PEFT method for SSM modules, supported by both theory and experiments.

2 Related Works

Parameter-Efficient Fine-Tuning (PEFT). As mentioned in Sec. 1, PEFT methods fall into three categories: (i) input-injected, (ii) architecture-enhanced, and (iii) weight-tuning approaches. Common input-injected methods include prompt tuning (Lester et al., 2021), which prepends learnable virtual tokens as continuous vectors, and prefix-tuning (Li & Liang, 2021), which extends this approach by adding tokens across the model’s depth for greater efficacy.¹ Architecture-enhanced methods modify the model architecture beyond operations on existing weights. For example, Houldsby et al. (2019) added layers between Transformer layers, while Additional-scan (Yoshimura et al., 2024) expands state dimensions in the SSM module. In contrast, weight-tuning methods directly operate on existing model weights. Recent advancements include Low-Rank Adaptation (LoRA) (Hu et al., 2021), which updates weight matrices using two smaller trainable matrices. Several variants have been proposed, such as LoRA+ (Hayou et al., 2024), which introduces differential learning rates, and DoRA (Liu et al., 2024), which incorporates a trainable scaling parameter. Another notable method, BitFit (Zaken et al., 2022) focuses exclusively on tuning bias terms. In Sec. A, we provide a more detailed discussion of these baseline methods.

Concurrent works of PEFT on SSMs. Several concurrent studies (Halloran et al., 2024; Yoshimura et al., 2024) have investigated PEFT methods for SSM-based models. Halloran et al. (2024) studied both in-context learning and parameter-efficient fine-tuning, with an orthogonal focus on analyzing Mamba’s stability under mixed-precision training using Lyapunov exponents. Yoshimura et al. (2024) benchmarked multiple PEFT approaches—including established methods and a new method called Additional-scan (which adds a state dimension to the SSM module), plus partial tuning (fine-tuning only a subset of parameters)—and introduced MambaPEFT through PEFT search strategies. While Yoshimura et al. (2024) solely focused on Mamba-I, providing an in-depth study of that particular architecture, our work investigates a broader class of SSM-based models including deep S4, Mamba-I, Jamba in the main body, as well as Mamba-II presented in Sec. C.2 and E.2, aiming to offer general insights on how to effectively tune SSMs rather than focusing on a single variant.

Sparse Tuning. Several studies have explored sparse parameter selection in fine-tuning (Song et al., 2023) and skill localization (Panigrahi et al., 2023). Song et al. (2023) showed that sparse tuning is an effective PEFT method, linking the low intrinsic dimensionality of pre-trained models to the proportion of parameters needing updates. They propose selecting optimal fine-tuning parameters based on gradient magnitudes. We enable sparse tuning for SSM by applying sparsity across entire dimensions (channel and state) rather than specific neurons. Panigrahi et al. (2023) focused on identifying neurons responsible for specific downstream tasks by fully fine-tuning the model and

¹In Yoshimura et al. (2024), prefix-tuning is referred to as “affix tuning” due to a implementation difference in SSM compared to standard Transformer models.

computing neuron masks to minimize task loss. While effective for skill localization, this method is computationally expensive and not optimized for parameter-efficient fine-tuning.

3 Preliminaries of State Space Models

Discrete-time SSMs. The initial SSM is derived from a specific continuous system that maps a one-dimensional function or signal $x(t) \in \mathbb{R}$ to $y(t) \in \mathbb{R}$ via an H -dimensional latent state $\mathbf{h}(t) \in \mathbb{R}^H$, as described in equation 1. In equation 1, input transition vector $\mathbf{B} \in \mathbb{R}^{H \times 1}$ indicates the input's impact on the state of the system, state matrix $\mathbf{A} \in \mathbb{R}^{H \times H}$ characterizes the system's internal state dynamics, and the output mapping vector $\mathbf{C} \in \mathbb{R}^{1 \times H}$ relates the state to the output $y(t)$.²

$$\begin{aligned} \mathbf{h}'(t) &= \mathbf{A}\mathbf{h}(t) + \mathbf{B}x(t) & (1) \\ y(t) &= \mathbf{C}\mathbf{h}(t) & \end{aligned} \quad \begin{aligned} \mathbf{h}_t &= \overline{\mathbf{A}}\mathbf{h}_{t-1} + \overline{\mathbf{B}}x_t, & (2) \\ y_t &= \mathbf{C}\mathbf{h}_t \end{aligned}$$

$$\begin{aligned} \overline{\mathbf{K}} &= (\mathbf{C}\overline{\mathbf{B}}, \mathbf{C}\overline{\mathbf{A}}\overline{\mathbf{B}}, \dots, \mathbf{C}\overline{\mathbf{A}}^{t-1}\overline{\mathbf{B}}), & (3) \\ (y_1, \dots, y_t) &= (x_1, \dots, x_t) * \overline{\mathbf{K}} \end{aligned}$$

To adapt SSMs for deep learning, the continuous parameters (\mathbf{A}, \mathbf{B}) are discretized into $(\overline{\mathbf{A}}, \overline{\mathbf{B}})$ using a learnable step size $\Delta \in \mathbb{R}$. A common discretization rule, the zero-order hold, defines $\overline{\mathbf{A}} = \exp(\Delta\mathbf{A})$, $\overline{\mathbf{B}} = (\Delta\mathbf{A})^{-1}(\exp(\Delta\mathbf{A}) - \mathbf{I}) \cdot \Delta\mathbf{B}$. The discrete-time SSM, given in equation 2, enables efficient inference via long convolution described in equation 3. For multi-channel inputs $\mathbf{x}, \mathbf{y} \in \mathbb{R}^D$, separate SSMs are used per channel, with a superscript (d) indicating channel-specific parameters when needed.

Structured State Space Sequence Model (S4). S4, introduced by Gu et al. (2022b), is an early application of SSMs in deep learning, featuring a *diagonal* state matrix \mathbf{A} . To introduce non-linearity and cross-channel mixing, S4 integrates a position-wise linear layer, activation function, and a residual connection from input to output. Let \otimes represent the element-wise product, and $\text{S4}(\cdot)$ denote the S4 mechanism, where each channel's output follows equation 3 with its convolutional kernel $\overline{\mathbf{K}}^{(d)}$. While the subtle details such as the activation functions may vary slightly from the previous studies (Gu et al., 2022b,a), for the theoretical analysis in this paper, we define the *deep S4 layer* as:

$$\mathbf{y}_t = \text{ReLU}(\mathbf{W} \cdot \text{S4}_t(\mathbf{x}_1, \dots, \mathbf{x}_t) + \boldsymbol{\beta} + \mathbf{u} \otimes \mathbf{x}_t), \quad (4)$$

where $\mathbf{W} \in \mathbb{R}^{D \times D}$ and $\boldsymbol{\beta} \in \mathbb{R}^D$ represent the linear projection matrix and bias, respectively, and $\mathbf{u} \in \mathbb{R}^D$ is the coefficient of the residual connection. Trainable parameters include SSM parameters $(\mathbf{A}^{(d)}, \mathbf{B}^{(d)}, \mathbf{C}^{(d)}, \Delta^{(d)})$ across D channels with $\mathbf{A}^{(d)}$ being diagonal, and $(\mathbf{W}, \boldsymbol{\beta})$ for the linear layer and \mathbf{u} for the residual connection.

Selective State Space Models (S6). All SSMs mentioned above exhibit linear time invariance (LTI), meaning their dynamics remain constant over time. A key limitation of LTI SSMs is their fixed dynamics, hindering selective context extraction and input-dependent state transitions. S6 (Gu & Dao, 2024) addresses this by making parameters input-dependent. At each time step t , given the input $\mathbf{x}_t \in \mathbb{R}^D$, S6 introduces input-dependent step size $\Delta_t = (\Delta_t^{(1)}, \dots, \Delta_t^{(D)})^\top \in \mathbb{R}^D$, input transition vectors $\mathbf{B}_t \in \mathbb{R}^{H \times 1}$ and the output mapping vectors $\mathbf{C}_t \in \mathbb{R}^{1 \times H}$ via linear projection:

$$\Delta_t = \text{softplus}(\mathbf{W}_\Delta \mathbf{x}_t + \boldsymbol{\beta}_\Delta), \quad \mathbf{B}_t = \mathbf{W}_B \mathbf{x}_t, \quad \mathbf{C}_t = \mathbf{W}_C \mathbf{x}_t,$$

where the diagonal state matrices $\mathbf{A}^{(1)}, \dots, \mathbf{A}^{(D)}$ remain input-independent. The weight $\mathbf{W}_\Delta \in \mathbb{R}^{D \times D}$ is factorized as $\mathbf{W}_\Delta = \mathbf{W}_{\Delta,\uparrow} \mathbf{W}_{\Delta,\downarrow}$, with $\mathbf{W}_{\Delta,\uparrow} \in \mathbb{R}^{D \times r}$, $\mathbf{W}_{\Delta,\downarrow} \in \mathbb{R}^{r \times D}$ to reduce computation (Wang et al., 2021, 2023a). Trainable parameters in S6 include $\mathbf{A}^{(d)}$ across D channels, $\mathbf{W}_{\Delta,\uparrow}, \mathbf{W}_{\Delta,\downarrow}$ and $\boldsymbol{\beta}_\Delta$ for computing Δ_t , and $\mathbf{W}_B, \mathbf{W}_C \in \mathbb{R}^{H \times D}$ for computing $\mathbf{B}_t, \mathbf{C}_t$. Discretization follows: $\overline{\mathbf{A}}_t^{(d)} = \exp(\Delta_t^{(d)} \mathbf{A}^{(d)})$, $\overline{\mathbf{B}}_t^{(d)} = \Delta_t^{(d)} \mathbf{B}_t$. Unlike S4, where $\mathbf{B}^{(d)}$ varies per channel, S6's variation on $\overline{\mathbf{B}}_t^{(d)}$ stems from the scalar $\Delta_t^{(d)}$. Additionally, S6 shares \mathbf{C}_t for all channels at each time step t , while S4 assigns a distinct $\mathbf{C}^{(d)}$ to each channel.

²Note that \mathbf{B}, \mathbf{C} are vectors; we use bold capitals for consistency with prior work. (Gu et al., 2022b; Gu & Dao, 2024).

Mamba & Jamba. Similar to the Transformer block, which consists of attention and linear layers, the Mamba-I block proposed by [Gu & Dao \(2024\)](#) features an S6 module, a point-wise 1D causal convolution layer (Conv1d) for token mixing, linear layers — including input (\mathbf{W}_{in}) and output (\mathbf{W}_{out}) projection layers and a gated MLP. Mamba-II ([Dao & Gu, 2024](#)) further simplifies the state matrix \mathbf{A} to be a scalar. Building on Mamba-I, Jamba ([Lieber et al., 2024](#)) introduces a hybrid architecture that integrates both Transformer blocks and Mamba blocks, leveraging the strengths of both to enhance performance. This paper focuses on Mamba-I (referred as Mamba in this paper) and Jamba, deferring Mamba-II discussions to the appendix.

4 Benchmarking PEFT Methods on SSM-based Models

In this section, we examine the effectiveness of popular PEFT methods when applied naively to SSM-based models, specifically Mamba and Jamba.

4.1 Experiment Setup

We evaluate PEFT methods across three categories: input-injected, architecture-enhanced, and weight-tuning. For input-injected methods, we use prompt tuning ([Lester et al., 2021](#)) and prefix-tuning ([Li & Liang, 2021](#)), where prefix-tuning employs an overparameterized MLP for stable optimization. For architecture-enhanced methods, we include additional-scan ([Yoshimura et al., 2024](#)), which introduces and fine-tunes newly added state dimensions in SSM modules. For weight-tuning, we consider BitFit ([Zaken et al., 2022](#)) and LoRA*, including LoRA ([Hu et al., 2021](#)) and DoRA ([Liu et al., 2024](#)), while LoRA+ ([Hayou et al., 2024](#)) is deferred to Sec. E.2. BitFit fine-tunes the bias terms of Conv1d and $\mathbf{W}_{\Delta,\uparrow}$.

We evaluate these methods on six datasets spanning different domains: GLUE for natural language understanding ([Wang et al., 2019](#)), DART for RDF-to-text generation ([Nan et al., 2021](#)), SAM-Sum ([Gliwa et al., 2019](#)) for summarization, Spider for text-to-SQL generation ([Yu et al., 2018](#)), and two vision datasets—CIFAR-10 ([Krizhevsky et al., 2009](#)) and CelebA ([Liu et al., 2015](#)). Details are in Sec. B. Prefix-tuning requires significantly more parameters than other PEFT methods due to its per-layer MLP for projecting fixed sequences into soft tokens. For all methods—except prefix-tuning, and except LoRA and DoRA when they are applied to both major components—we limit trainable parameters to below 1% for Mamba and below 0.15% for Jamba. For Jamba, all PEFT methods are applied to Mamba layers, while Transformer layers remain frozen to isolate performance effects.

4.2 Results

Table 1 presents the benchmarking results. Detailed results for different subtasks in GLUE and Spider can be found in Sec. C.2. We analyze the results from three aspects below.

Limitations of Input-Injected Method. Input-injected methods like prefix-tuning are ineffective for SSM-based models (Table 1), as their expressiveness reduces to tuning only the initial hidden state (Proposition 1). Formal statement, proof and empirical verification are in Sec. C.3.

Optimal Application of LoRA* in SSM-based Models. Table 1 shows that LoRA* outperforms all other PEFT methods in most scenarios. From our results, we explore the optimal layers for applying LoRA* in SSM-based models: the SSM module, the linear projection matrices, or a combination of both. Note that S6 in Mamba and Jamba includes fine-grained parameters like \mathbf{x}_{proj} ($\mathbf{W}_B, \mathbf{W}_C, \mathbf{W}_{\Delta,\downarrow}$) and $\mathbf{dt}_{\text{proj}}$ ($\mathbf{W}_{\Delta,\uparrow}$), which were already explored by [Yoshimura et al. \(2024\)](#) on Mamba. We defer a deeper discussion of them to Sec. C.4 and focus on the key question: Is applying LoRA* to SSM modules necessary for performance gains? By narrowing our scope, we aim to clarify LoRA*'s impact across different components.

We evaluate LoRA*'s performance on linear projections using \mathbf{W}_{in} , \mathbf{W}_{out} , and both combined. Since the performance of different combinations of linear projections is consistent across datasets (see Sec. C.4.), we only report the results for LoRA* applied to \mathbf{W}_{in} in Table 1. For SSM modules, we apply LoRA* to weight matrices, including those for the input-dependent step size Δ . For state transition matrices \mathbf{A} , we treat their diagonal structures as vectors, concatenate them across

| Model | Method | Major Target Module | GLUE | | DART | | SAMSum | | | Spider | CIFAR-10 | CelebA |
|-------|------------------|---------------------|-------------|-------------|-------------|-------------|-------------|-------------|-------------|-------------|-------------|--------|
| | | | Avg. Score | METEOR | BLEU | R1 | R2 | RL | Acc. | Acc. | Acc. | Acc. |
| Mamba | Prompt Tuning | Other | 63.8 | 66.2 | 39.8 | 50.1 | 25.6 | 41.6 | 43.6 | 30.4 | 82.5 | |
| | Prefix-Tuning | SSM | 68.6 | 66.6 | 42.5 | 50.6 | 26.5 | 42.1 | 39.7 | 41.0 | 86.5 | |
| | BitFit | Both | 76.8 | 67.0 | 43.7 | 50.3 | 25.7 | 41.9 | 48.4 | 44.4 | 86.9 | |
| | LoRA | SSM | 76.9 | 68.8 | 48.0 | 50.4 | 26.0 | 41.8 | 55.0 | 52.3 | 87.0 | |
| | | LinProj | 81.2 | 70.9 | 49.5 | 50.9 | 27.0 | 42.3 | 57.5 | 61.0 | 87.0 | |
| | | Both | 80.3 | 70.2 | 52.2 | 50.7 | 26.8 | 42.4 | 57.0 | 58.4 | 89.8 | |
| | DoRA | SSM | 77.9 | 68.3 | 47.3 | 48.1 | 24.2 | 39.6 | 55.3 | 44.5 | 87.1 | |
| | | LinProj | <u>81.1</u> | 70.7 | 51.6 | <u>51.0</u> | 26.9 | 42.8 | 60.7 | 57.6 | 86.7 | |
| | | Both | 80.8 | <u>70.8</u> | 51.4 | 51.3 | 27.2 | 43.0 | <u>58.1</u> | 58.2 | 89.8 | |
| Jamba | Additional-Scan | SSM | 62.4 | 60.6 | 15.8 | 37.6 | 17.5 | 30.9 | 26.9 | 32.2 | 86.0 | |
| | Full Fine-Tuning | Both | 80.5 | 71.0 | 51.8 | 51.2 | 27.3 | 42.9 | 66.2 | 60.0 | 89.4 | |
| | Prompt Tuning | Other | 73.3 | 54.1 | 6.3 | 54.7 | 31.8 | 46.8 | 74.9 | 40.9 | 85.6 | |
| | Prefix-Tuning | SSM | 56.9 | 59.6 | 14.4 | 11.5 | 1.8 | 10.4 | 0.3 | 29.9 | 82.2 | |
| | BitFit | Other | 75.2 | 59.2 | 14.8 | <u>54.7</u> | 31.9 | <u>47.0</u> | <u>73.7</u> | 45.6 | 86.3 | |
| | LoRA | LinProj | <u>73.9</u> | 68.9 | 37.8 | 54.6 | 32.3 | 46.8 | 69.3 | 59.7 | 89.0 | |
| | DoRA | LinProj | 71.4 | <u>68.1</u> | <u>28.8</u> | 55.2 | <u>32.2</u> | 47.3 | 70.9 | <u>58.6</u> | 89.0 | |
| | Additional-Scan | SSM | 68.3 | 63.3 | 20.1 | 53.4 | 30.5 | 45.6 | 69.3 | 50.6 | 0.0 | |

Table 1: **Benchmarking popular Parameter-Efficient Fine-Tuning (PEFT) methods on Mamba (Gu & Dao, 2024) and Jamba (Lieber et al., 2024) across six real-world datasets.** R1/R2/RL stand for ROUGE-1/2/L. We evaluate PEFT applied to different target modules: SSM module only, linear projection matrices (LinProj) only, both, or other components such as embedding layer. For both Mamba and Jamba, all methods use fewer than 1% and 0.15% of parameters, respectively, except when the target module for LoRA or DoRA is set to “Both” or when prefix-tuning is applied. Comprehensive hyperparameter tuning was performed for all methods. Bold values indicate the best performance for each model (Mamba and Jamba) separately, while underlined values denote the second-best performance for each task, excluding full fine-tuning. Key findings include: (i) among PEFT methods applied to SSM modules, LoRA* outperforms others, (ii) for all PEFT methods, LoRA* achieves the best performance, (iii) applying LoRA* to linear projections yields results comparable to applying it to both linear projections and SSM modules, while outperforming its application solely to SSM modules, and (iv) input-injected methods (i.e., prompt tuning and prefix tuning), are generally ineffective.

channels to form a matrix, and apply LoRA*. Table 1 summarizes results for the best-performing configurations (see Sec. C.2 for full results). Based on these results, we derive the following findings:

Finding: *For LoRA*: Tuning on SSMs is less effective than tuning linear projection matrices, with the latter performing comparably to tuning both.*

Detailed experiments, including LoRA* on different linear projection matrices and additional evaluations of LoRA+ and Mamba-II, are presented in Sec. E.2. These experiments reinforce the finding that LoRA* is highly effective for linear projections but less suitable for SSM modules.

To further elucidate this concept, we present the following lemma, which examines a simplified model architecture consisting of S6 with a linear input projection matrix at each layer. We demonstrate that fine-tuning the projection matrix \mathbf{W}_{in} encompasses the expressivity of fine-tuning the parameters \mathbf{W}_B , \mathbf{W}_C , and $\mathbf{W}_{\Delta,\uparrow}$.

Lemma 1 (Expressivity of Fine-Tuning Projection Matrices). *Consider an S6 with an additional linear input projection matrix \mathbf{W}_{in} . Denote the input-dependent SSM parameters $\{\{\overline{\mathbf{A}}_n^{(d)}\}_{d=1}^D, \overline{\mathbf{B}}_n, \mathbf{C}_n\}_{n=1}^N$ as $\theta(\cdot; \{\mathbf{A}^{(d)}\}_{d=1}^D, \mathbf{W}_B, \mathbf{W}_C, \mathbf{W}_{\Delta,\uparrow}, \mathbf{W}_{\Delta,\downarrow}, \mathbf{W}_{in})$. For any given $\overline{\mathbf{W}}_B$, $\overline{\mathbf{W}}_C$, and $\overline{\mathbf{W}}_{\Delta,\uparrow}$, there exists a $\widehat{\mathbf{W}}_{in}$ such that for any input sequences $\mathbf{X} \in \mathbb{R}^{D \times N}$,*

$$\theta(\mathbf{X}; \{\mathbf{A}^{(d)}\}_{d=1}^D, \overline{\mathbf{W}}_B, \overline{\mathbf{W}}_C, \overline{\mathbf{W}}_{\Delta,\uparrow}, \mathbf{W}_{\Delta,\downarrow}, \mathbf{W}_{in}) = \theta(\mathbf{X}; \{\mathbf{A}^{(d)}\}_{d=1}^D, \mathbf{W}_B, \mathbf{W}_C, \mathbf{W}_{\Delta,\uparrow}, \mathbf{W}_{\Delta,\downarrow}, \widehat{\mathbf{W}}_{in}).$$

We expand on this discussion in Sec. C.4, where we provide a more detailed statement of the above assertion along with its corresponding proofs. This raises an important question: does this imply that fine-tuning SSM modules is unnecessary? We argue that this is not the case. Key parameters beyond \mathbf{W}_B , \mathbf{W}_C , and $\mathbf{W}_{\Delta,\uparrow}$, such as the state matrix \mathbf{A} and $\mathbf{W}_{\Delta,\downarrow}$, remain crucial. In particular, \mathbf{A} plays

a critical role in sequence-to-sequence operations. However, Table 1 shows that applying LoRA* to SSM modules does not improve performance. Intuitively, fine-tuning these additional parameters should enhance the model’s expressive power. To explore this further, we examine the applicability of various PEFT methods to SSM modules, including LoRA*, prefix-tuning, and additional-scan. Our comparisons in Table 1 reveal that:

Finding: *For SSMs, LoRA* outperforms other existing PEFT methods.*

This raises a key question: is there a more effective approach for fine-tuning SSM modules?

5 Sparse Dimension Tuning

This section aims to develop an algorithm for tuning SSM modules. In doing so, we start by first analyzing the roles of different parameters, as outlined in Lemma 2. This analysis motivates us to classify channels and state dimensions into three categories: (i) zero, (ii) trainable, and (iii) frozen, leading to the development of the *Sparse Dimension Tuning and Pruning* (SDT-P) method. We then establish theoretical guarantees for applying SDT-P to SSM modules and LoRA to linear projection matrices (Theorem 1). Finally, we simplify SDT-P into *Sparse Dimension Tuning* (SDT) by omitting pruning, as pruned parameters can be effectively considered as being trained to zero. This simplified version serves as the primary method used in our experiments.

5.1 Understanding Key Parameters in S4 Modules

Problem Setting. Inspired by the work by [Zeng & Lee \(2024\)](#), we analyze the expressive power of S4 parameters using a similar framework. We assume a well-performing target model and a frozen model (pretrained or random) and aim to update the frozen model efficiently to match the target. Following [Zeng & Lee \(2024\)](#), we assume the frozen model has a capacity at least equal to the target model, ensuring (i) analytical traceability and (ii) practical relevance due to model overparameterization. Both models are S4 with hidden dimensions H_* (target) and $H \geq H_*$ (frozen). Assuming all hidden dimensions are active, we define their dynamics using discretized parameters $(\bar{A}, \bar{B}, \bar{C})$:

$$\begin{aligned} \text{(Target model)} \quad f^*(\mathbf{x})_n &= \sum_{m=1}^n \bar{C}_* \bar{A}_*^{m-n} \bar{B}_* x_m, \\ \text{(Frozen model)} \quad f_0(\mathbf{x})_n &= \sum_{m=1}^n \bar{C}_0 \bar{A}_0^{m-n} \bar{B}_0 x_m, \end{aligned}$$

where $\text{diag}(\bar{A}_*), \bar{B}_* \in \mathbb{R}^{H_*}$, $\text{diag}(\bar{A}_0), \bar{B}_0, \bar{C}_0 \in \mathbb{R}^H$. The formulation shows that the S4 module remains unchanged even if the state dimensions are permuted.

Parameter Efficiency Analysis on S4. We analyze the parameter efficiency of the S4 model after the necessary discretization of its parameters $(\bar{A}_0, \bar{B}_0, \bar{C}_0)$. Let Θ_0 be the set of parameters $(\bar{A}_0, \bar{B}_0, \bar{C}_0)$ up to the same permutation. Given this formulation, we present our first analysis of parameter efficiency for the S4 model as below.

Lemma 2 (Minimal Parameter Adjustment for S4 Fine-Tuning). *To update frozen model f_0 such that it becomes functionally equivalent to the target model f^* , the minimum number of tunable parameters is:*

$$\min_{(\bar{A}, \bar{B}, \bar{C}) \in \Theta_0} \overbrace{\left\| [\text{diag}(\bar{A}) \otimes \bar{B} \otimes \bar{C}^\top]_{(H_*+1):H} \right\|_0}^{\text{eliminating redundant dimensions}} + \overbrace{\left\| [\bar{A}]_{1:H_*, 1:H_*} - \bar{A}_* \right\|_0 + \left\| [\bar{B} \otimes \bar{C}^\top]_{1:H_*} - \bar{B}_* \otimes \bar{C}_*^\top \right\|_0}^{\text{aligning remaining dimensions with target model}}. \quad (5)$$

Proofs and further details are provided in Sec. D.1. This result highlights three distinct roles of the state dimensions. First, any dimensions that do not contribute to the target function (represented by the first term in equation 5) are effectively zero and can be pruned. These correspond to state dimensions larger than those of the target model after permutation, indicating that redundant information can be directly removed to eliminate its impact. Second, among the remaining dimensions, alignment is necessary for those that do not already match the target. The state matrix A plays a crucial role in sequence modeling by capturing dependencies between tokens at different positions. To achieve functional equivalence (as represented by the second term in equation 5), A must be aligned. Notably,

dimensions that are already aligned with the target require no updates. These two insights motivate our Sparse Dimension Tuning and Pruning (SDT-P) method, which classifies hidden dimensions into three categories: (i) zero, (ii) frozen (already aligned), and (iii) trainable. Finally, the third term in equation 5 indicates that the expressive power of \bar{B} and C is essentially equivalent, meaning that tuning either one is sufficient.

5.2 Sparse Dimension Tuning and Pruning (SDT-P)

Building on Lemma 2, we introduce SDT-P, the precursor to Sparse Dimension Tuning (SDT). SDT-P updates parameters selectively based on the role of each state dimension. In the multi-channel case, we first categorize the channel dimensions into three groups: pruned, frozen, and trainable. Then, the state dimensions of each trainable channel are also categorized as pruned, frozen, or trainable. This hierarchical selection ensures that updates are applied only when necessary, while pruned dimensions are discarded and frozen dimensions remain unchanged.

Dimension Selection Algorithm. To enable this structured tuning process, we first introduce our dimension selection algorithm. The algorithm starts with a warmup epoch, where the SSM modules are updated using a subset of the dataset for one epoch. After this warmup, we classify channel dimensions based on the magnitude of the state matrix A : dimensions with small magnitude are pruned (set to zero), those with significant changes are marked as trainable, and the rest remain frozen. Next, we apply the same classification to state dimensions, but only within the trainable channels. The detailed pseudo-code is in Alg. 2.

Parameter Update Scheme. Once the channel and state dimensions are selected, we determine how to update the parameters. **(S4)** For S4, Gu et al. (2022a) showed that tuning \bar{C} alone is as effective as tuning both \bar{B} and C . Therefore, we always freeze \bar{B} and update only \bar{A} and C . Specifically, an entry in \bar{A} or C is trainable if and only if both its channel and state dimensions are trainable. If either the channel or state dimension is pruned, the entry is pruned as well. All other entries remain frozen. **(S6)** For S6, where parameters are input-dependent, we update \bar{A} , W_B , and W_C instead. Since W_B and W_C operate across channels, we categorize their updates based only on channel dimensions—we do not update individual state dimensions differently for each channel. Based on this categorization, we mark the corresponding columns of W_B and W_C as trainable, frozen, or pruned accordingly.

The dimension selection algorithm and parameter updates together form the SDT-P method for tuning SSM modules. Next, we provide theoretical guarantees for applying SDT-P to SSM modules and LoRA* to linear projection matrices.

5.3 Expressive Power of SDT-P Combined with LoRA

We consider cases where each input token $x_t \in \mathcal{X}$ is bounded in \mathbb{R}^D , and the input sequence length is finite. Our analysis focuses on simplified SSM-based models, where each layer consists of an SSM module followed by linear projection matrices with residual connections. We refer to this structure as a deep SSM layer: i) a deep S4 layer consists of an S4 module followed by linear projections; ii) a deep S6 layer follows the same structure but replace S4 with S6. A deep S4 model is composed of deep S4 layers, while a deep S6 model consists of deep S6 layers. The detailed formulation of deep S4 layers is provided in Sec. 3, and a deep S6 layer follows the same structure with S4 replaced by S6. The following theorem highlights the expressive capacity of SDT-P on simplified SSM-based models, where each layer uses a single type of SSM module (S4 or S6) followed by linear projection matrices. For proof and details, refer to Sec. D.3.1 and D.3.2.

Theorem 1 (Expressive Power of SDT-P Combined with LoRA on Simplified SSM-based Models). *Consider a D -dimensional input sequence and assume the model’s linear layers have linear activation functions. Using the following fine-tuning method:*

1. **(SDT-P on SSM)** Selectively fine-tuning and pruning at most $\lceil DL^*/L \rceil$ channels and H^* hidden states in SSM modules,
2. **(LoRA* on Linear Projections)** Applying rank- $\lceil L/L^* \rceil$ updates to the linear projection matrices, and
3. **(Minimal Updates to Additional Parameters)** Updating residual connections, biases at each layer, and the linear projection matrix in the last layer only,

any deep S4 or S6 model with H hidden states per channel and L layers can be adapted to accurately represent a target model of the same type (S4 or S6) without residual connections, with a reduced hidden state dimension $H^* < H$ and fewer layers $L^* < L$.

This theorem demonstrates that a larger pretrained model requires selecting fewer channels and hidden states at each layer. Furthermore, if the target task is less complex — evidenced by a smaller target model with fewer layers L^* and hidden states H^* — the number of channels and hidden states needed is also reduced. This finding aligns with the theoretical analysis of LoRA presented in [Zeng & Lee \(2024\)](#), which shows that larger pretrained models require fewer learnable parameters (referred to as “lower rank” in their context) during fine-tuning, especially for simpler tasks. Although this theorem is constrained by the assumptions of linear activations and the absence of residual connections in the target model, while also requiring fully fine-tuning the linear project matrix of last layer, our findings have broader implications. As our experimental results in Sec. 6 will show, these insights generalize beyond these theoretical constraints.

Algorithm 1: Dimension Selection Algorithm of SDT

Input: A small subset of Dataset \mathcal{D} , warmup epochs E , number of layers L , total channels D , total states H , channel freeze ratio α , state freeze ratio β

```

/* Warmup Epochs
Perform full update on SSM modules using  $\mathcal{D}$  for  $E$  epochs;
for  $l = 1$  to  $L$  do
    /* Unfreeze dimensions
    Sort channels  $\mathbb{D}$  based on changes of  $\|\bar{\mathbf{A}}^{(d)}\|$ ;
    Freeze the bottom  $\beta|\mathbb{D}|$  channels, denoted by  $\mathbb{D}'$ ;
    for  $d \in \mathbb{D}'$  do
        /* Sort state dimensions by the changes in  $\|\bar{\mathbf{A}}^{(d)}\|$ ;
        Freeze the bottom  $\alpha|\mathbb{H}|$  state dimensions at the  $d$ -th channel;

```

5.4 Sparse Dimension Tuning (SDT): A Pruning-Free Alternative

While SDT-P classifies channels and states into three categories, we simplify our approach by omitting pruning and categorizing parameters as either trainable or frozen. We refer this simplified method as *Sparse Dimension Tuning* (SDT). This reduces the number of hyperparameters, as pruned parameters are effectively equivalent to being trained to zero. The resulting dimension selection approach is outlined in the pseudo-code (Alg. 1), which corresponds to the update scheme illustrated in Fig. 1. Experiments will show that this simplification remains effective.

Overhead Analysis. We assess the computational overhead of applying SDT with LoRA (for linear projection matrices) versus LoRA alone with Table 2 summarizing the results. Although SDT involves an additional dimension selection stage, Table 2 shows that this incurs minimal extra cost. Furthermore, with the same parameter budget, SDT for SSM modules combined with LoRA on linear projections runs faster than LoRA alone, since LoRA introduces extra matrix multiplications between two low-rank matrices for the SSM modules, whereas SDT does not. In Sec. D.4, we detail the experimental settings and present a memory usage analysis showing that SDT also consumes less memory during fine-tuning for the same reason.

| Stage | Method | Mamba-130M | Mamba-1.4B | Jamba-Mini-52B |
|----------------------|------------|------------------|--------------------|--------------------|
| Dim. Selection | LoRA & SDT | 16.5 ± 3.9 | 85.8 ± 5.3 | 163.9 ± 10.2 |
| Training (per epoch) | LoRA | 410.0 ± 80.0 | 2060.0 ± 135.0 | 3427.5 ± 185.0 |
| | LoRA & SDT | 330.0 ± 77.5 | 1697.5 ± 87.5 | 3065.0 ± 232.5 |

Table 2: **PEFT combining SDT with LoRA is more efficient than LoRA alone when the same number of trainable parameters are used.** Shown are dimension selection and per-epoch training times (s) for Mamba and Jamba models.

6 Experimental Studies of SDT

In this section, we evaluate the performance of SDT in tuning SSM modules, comparing it to LoRA*, the best existing PEFT method for fine-tuning SSM modules, as shown in Sec. 4. Our experiments reveal the key result:

Finding: *SDT outperforms LoRA* on SSM modules.*

6.1 Synthetic Experiments on Deep S4 Models

This experiment validates our theoretical guarantees under broader conditions, including residual connections and ReLU activations in both models, without fully fine-tuning the last-layer projection matrix. See Sec. E.1 for details.

(Experiment Setup) We employ a regression setting to validate our theoretical results. We randomly initialize two models: a one-layer deep S4 model as the target and a four-layer deep S4 model as the frozen model. LoRA is applied to linear projection matrices, while different methods are tested on the SSM module to assess their effectiveness. The goal is to update the frozen model to match the target model’s functionality. We generate an input sequence \mathbf{X} of length 200 and dimension 64, with values uniformly drawn from integers between 0 and 9. This input is then processed through the target model to obtain the corresponding outputs. These input-output pairs are used to train the frozen model over 500 iterations using the Mean Squared Error (MSE) loss. **(Results)** Figure 2 shows the MSE, averaged across all tokens, plotted against the number of trainable parameters for different methods on SSM modules. SDT achieves significantly lower MSE than LoRA on SSM modules, demonstrating its effectiveness.

6.2 Real-World Experiments on Pretrained Models

Lastly, we conduct experiments to evaluate our approach on pretrained models, including Mamba and Jamba with different model sizes. We consider five datasets: GLUE, DART, SAMSum, Spider, and CelebA. For these experiments, we split the datasets into three parts: train, validation, and test, different from benchmarking experiments. We combine our proposed SDT with LoRA* and evaluate it in three different settings against three pure LoRA* settings. In SDT, 99% of channels are frozen, and we adjust state freeze ratios. For the pure LoRA* settings, we apply LoRA* to different parameter sets, selecting ranks to ensure all settings have a comparable parameter budget for fair comparison. Residual connections and biases are frozen and learning rates are independently selected via a small grid search over data subsets. See Sec. E.2 for further details.

Mamba. The experimental results of Mamba are reported in Table 3, showing that applying SDT on SSM modules outperforms pure LoRA*, even when 99% of the channels are frozen. This underscores the effectiveness of SDT on fine-tuning SSM modules.

Jamba. We extend our experiments to Jamba, applying all tested methods exclusively to its Mamba layers. Notably, the performance gain on Jamba is smaller compared to Mamba. This is because we freeze all Transformer layers to isolate the effect of Mamba layers for a fair evaluation. Additionally, since the Mamba layers in Jamba contain significantly fewer parameters than those in the Mamba model, fine-tuning them yields limited performance improvements. Nevertheless, results on GLUE (Table 4) validate the effectiveness of our method. See Table 21 for more results.

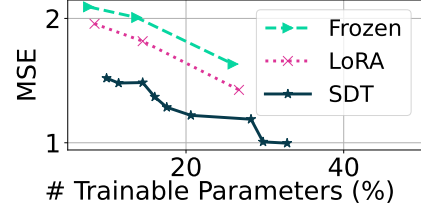


Figure 2: SDT outperforms LoRA in tuning S4 within deep S4 models when LoRA is applied to linear projection matrices in synthetic experiments.

| LinProj | S6 | GLUE | | DART | | CelebA | | SAMSum | | Spider | |
|---------|------|-------------|-------------|-------------|-------------|-------------|-------------|-------------|-------------|--------|--|
| | | Avg. | BLEU | MET. | Acc. | R1 | R2 | RL | Acc. | | |
| LoRA | LoRA | 80.8 | 51.0 | 70.2 | 88.6 | 51.6 | 28.2 | 43.2 | 83.5 | | |
| | SDT | 81.1 | 51.5 | 70.5 | 88.6 | 51.7 | 28.1 | 43.4 | 84.5 | | |
| DoRA | DoRA | 80.1 | 51.2 | 70.4 | 88.4 | 51.8 | 28.0 | 43.4 | 83.8 | | |
| | SDT | 78.2 | 51.5 | 70.8 | 88.6 | 52.1 | 28.3 | 43.7 | 85.1 | | |

Table 3: **Performance comparison between SDT and LoRA on pretrained Mamba models.** **Bold** numbers indicate the best performance for each task. We use Mamba-130M to compare the performance of SDT and LoRA on GLUE (Wang et al., 2019), DART (Nan et al., 2021), and CelebA (Liu et al., 2015) benchmarks. For all other datasets, we employ Mamba-1.4B. We report only the best setting out of three for each method. We observe that SDT outperforms LoRA* on updating SSM modules on Mamba.

| LinProj | S6 | RTE | MRPC | CoLA | SST-2 | QNLI | QQP | MNLI | Avg. |
|---------|------|-------------|-------------|------------|-------------|-------------|-------------|-------------|-------------|
| DoRA | DoRA | 65.7 | 77.8 | 7.1 | 93.9 | 77.8 | 67.8 | 85.4 | 67.9 |
| | SDT | 67.1 | 77.5 | 7.5 | 94.2 | 79.6 | 72.7 | 85.5 | 69.2 |

Table 4: **Performance comparison between SDT and DoRA on pretrained Jamba models.** **Bold** numbers indicate the best performance for each task. We use Jamba-Tiny-319M to compare the performance of SDT and DoRA on the GLUE (Wang et al., 2019) benchmark. We report only the best setting out of three for each method. We observe that SDT outperforms DoRA on updating SSM modules on Jamba.

7 Discussion

In this paper, we study the performance of PEFT methods applied to SSM-based models. Our evaluation of existing PEFT methods provides valuable insights and guidelines for future researchers to parameter-efficiently fine-tune SSM-based models for other domains. Moreover, we take an initial step in establishing a theoretical framework for studying PEFT methods on SSM-based models. Additionally, we introduce SDT, a novel PEFT method specifically tailored to SSM modules, demonstrating superior performance compared to existing approaches.

Limitations & Future Works. While our work provides valuable insights, certain limitations remain. The theoretical guarantees for SDT are restricted to linear activations and require full fine-tuning of the last layer. Nonetheless, our experiments show that SDT performs well in practice despite these constraints. Addressing these theoretical limitations or developing new PEFT methods applicable to broader scenarios is a promising future direction. Additionally, our theory shows that modifying a subset of channels and states is sufficient but does not guide optimal selection. Our approach, based on a warmup stage and parameter magnitude, might not be optimal. Future research could explore the impact of channel/state selection and improve dimension selection algorithms.

Acknowledgment

The work of Kangwook Lee is supported in part by NSF CAREER Award CCF-2339978, Amazon Research Award, and a grant from FuriosaAI.

References

Josh Achiam, Steven Adler, Sandhini Agarwal, Lama Ahmad, Ilge Akkaya, Florencia Leoni Aleman, Diogo Almeida, Janko Altenschmidt, Sam Altman, Shyamal Anadkat, et al. GPT-4 technical report. *arXiv preprint arXiv:2303.08774*, 2023.

Tom Brown, Benjamin Mann, Nick Ryder, Melanie Subbiah, Jared D Kaplan, Prafulla Dhariwal, Arvind Neelakantan, Pranav Shyam, Girish Sastry, Amanda Askell, et al. Language models

are few-shot learners. In *Advances in Neural Information Processing Systems*, volume 33, pp. 1877–1901, 2020.

Tri Dao and Albert Gu. Transformers are SSMs: Generalized models and efficient algorithms through structured state space duality. In *International Conference on Machine Learning*, 2024.

Tuan Dinh, Yuchen Zeng, Ruisu Zhang, Ziqian Lin, Michael Gira, Shashank Rajput, Jyong Sohn, Dimitris Papailiopoulos, and Kangwook Lee. LIFT: Language-interfaced fine-tuning for non-language machine learning tasks. In *Advances in Neural Information Processing Systems*, 2022.

Daniel Y Fu, Tri Dao, Khaled Kamal Saab, Armin W Thomas, Atri Rudra, and Christopher Ré. Hungry hungry hippos: Towards language modeling with state space models. In *International Conference on Learning Representations*, 2022.

Angeliki Giannou, Shashank Rajput, and Dimitris Papailiopoulos. The expressive power of tuning only the normalization layers. In *The Thirty Sixth Annual Conference on Learning Theory*, pp. 4130–4131, 2023.

Bogdan Gliwa, Iwona Mochol, Maciej Biesek, and Aleksander Wawer. SAMSum corpus: A human-annotated dialogue dataset for abstractive summarization. *EMNLP-IJCNLP 2019*, pp. 70, 2019.

Albert Gu and Tri Dao. Mamba: Linear-time sequence modeling with selective state spaces. In *First Conference on Language Modeling*, 2024.

Albert Gu, Tri Dao, Stefano Ermon, Atri Rudra, and Christopher Ré. Hippo: Recurrent memory with optimal polynomial projections. In *Advances in Neural Information Processing Systems*, volume 33, pp. 1474–1487, 2020.

Albert Gu, Isys Johnson, Karan Goel, Khaled Saab, Tri Dao, Atri Rudra, and Christopher Ré. Combining recurrent, convolutional, and continuous-time models with linear state space layers. In *Advances in Neural Information Processing Systems*, volume 34, pp. 572–585, 2021.

Albert Gu, Karan Goel, Ankit Gupta, and Christopher Ré. On the parameterization and initialization of diagonal state space models. In *Advances in Neural Information Processing Systems*, volume 35, pp. 35971–35983, 2022a.

Albert Gu, Karan Goel, and Christopher Ré. Efficiently modeling long sequences with structured state spaces. In *International Conference on Learning Representations*, 2022b.

Ankit Gupta, Albert Gu, and Jonathan Berant. Diagonal state spaces are as effective as structured state spaces. *Advances in Neural Information Processing Systems*, 35:22982–22994, 2022.

John T Halloran, Manbir Gulati, and Paul F Roysdon. Mamba state-space models can be strong downstream learners. *arXiv preprint arXiv:2406.00209*, 2024.

Soufiane Hayou, Nikhil Ghosh, and Bin Yu. Lora+: Efficient low rank adaptation of large models. *arXiv preprint arXiv:2402.12354*, 2024.

Junxian He, Chunting Zhou, Xuezhe Ma, Taylor Berg-Kirkpatrick, and Graham Neubig. Towards a unified view of parameter-efficient transfer learning. In *International Conference on Learning Representations*, 2021.

Neil Houlsby, Andrei Giurgiu, Stanislaw Jastrzebski, Bruna Morrone, Quentin De Laroussilhe, Andrea Gesmundo, Mona Attariyan, and Sylvain Gelly. Parameter-efficient transfer learning for NLP. In *International Conference on Machine Learning*, pp. 2790–2799, 2019.

Edward J Hu, Phillip Wallis, Zeyuan Allen-Zhu, Yuanzhi Li, Shean Wang, Lu Wang, Weizhu Chen, et al. LoRA: Low-rank adaptation of large language models. In *International Conference on Learning Representations*, 2021.

Zhiqiang Hu, Lei Wang, Yihuai Lan, Wanyu Xu, Ee-Peng Lim, Lidong Bing, Xing Xu, Soujanya Poria, and Roy Lee. LLM-adapters: An adapter family for parameter-efficient fine-tuning of large language models. In *Proceedings of the 2023 Conference on Empirical Methods in Natural Language Processing*, pp. 5254–5276, 2023.

Uijeong Jang, Jason D Lee, and Ernest K Ryu. LoRA training in the ntk regime has no spurious local minima. In *International Conference on Machine Learning*, 2024.

Angelos Katharopoulos, Apoorv Vyas, Nikolaos Pappas, and François Fleuret. Transformers are RNNs: Fast autoregressive transformers with linear attention. In *International Conference on Machine Learning*, pp. 5156–5165, 2020.

Alex Krizhevsky, Geoffrey Hinton, et al. Learning multiple layers of features from tiny images. 2009.

Brian Lester, Rami Al-Rfou, and Noah Constant. The power of scale for parameter-efficient prompt tuning. In *Proceedings of the 2021 Conference on Empirical Methods in Natural Language Processing*, pp. 3045–3059, 2021.

Xiang Lisa Li and Percy Liang. Prefix-Tuning: Optimizing Continuous Prompts for Generation. In *Proceedings of the 59th Annual Meeting of the Association for Computational Linguistics and the 11th International Joint Conference on Natural Language Processing (Volume 1: Long Papers)*, pp. 4582–4597, 2021.

Opher Lieber, Barak Lenz, Hofit Bata, Gal Cohen, Jhonathan Osin, Itay Dalmedigos, Erez Safahi, Shaked Meirom, Yonatan Belinkov, Shai Shalev-Shwartz, et al. Jamba: A hybrid transformer-mamba language model. *arXiv preprint arXiv:2403.19887*, 2024.

Shih-Yang Liu, Chien-Yi Wang, Hongxu Yin, Pavlo Molchanov, Yu-Chiang Frank Wang, Kwang-Ting Cheng, and Min-Hung Chen. Dora: Weight-decomposed low-rank adaptation. In *Proceedings of the 41st International Conference on Machine Learning*, volume 235, pp. 32100–32121, 2024.

Xiao Liu, Yanan Zheng, Zhengxiao Du, Ming Ding, Yujie Qian, Zhilin Yang, and Jie Tang. GPT Understands, Too. *arXiv:2103.10385*, 2021.

Xiao Liu, Kaixuan Ji, Yicheng Fu, Weng Tam, Zhengxiao Du, Zhilin Yang, and Jie Tang. P-Tuning: Prompt Tuning Can Be Comparable to Fine-tuning Across Scales and Tasks. In *Proceedings of the 60th Annual Meeting of the Association for Computational Linguistics (Volume 2: Short Papers)*, pp. 61–68, 2022.

Ziwei Liu, Ping Luo, Xiaogang Wang, and Xiaou Tang. Deep learning face attributes in the wild. In *Proceedings of the IEEE international conference on computer vision*, pp. 3730–3738, 2015.

Linyong Nan, Dragomir Radev, Rui Zhang, Amrit Rau, Abhinand Sivaprasad, Chiachun Hsieh, Xiangru Tang, Aadit Vyas, Neha Verma, Pranav Krishna, et al. DART: Open-Domain Structured Data Record to Text Generation. In *Proceedings of the 2021 Conference of the North American Chapter of the Association for Computational Linguistics: Human Language Technologies*, pp. 432–447, 2021.

Samet Oymak, Ankit Singh Rawat, Mahdi Soltanolkotabi, and Christos Thrampoulidis. On the role of attention in prompt-tuning. In *International Conference on Machine Learning*, pp. 26724–26768, 2023.

Abhishek Panigrahi, Nikunj Saunshi, Haoyu Zhao, and Sanjeev Arora. Task-specific skill localization in fine-tuned language models. In *International Conference on Machine Learning*, pp. 27011–27033, 2023.

Jongho Park, Jaeseung Park, Zheyang Xiong, Nayoung Lee, Jaewoong Cho, Samet Oymak, Kang-wook Lee, and Dimitris Papailiopoulos. Can Mamba learn how to learn? a comparative study on in-context learning tasks. In *International Conference on Machine Learning*, pp. 39793–39812, 2024.

Bo Peng, Eric Alcaide, Quentin Gregory Anthony, Alon Albalak, Samuel Arcadinho, Stella Biderman, Huanqi Cao, Xin Cheng, Michael Nguyen Chung, Leon Derczynski, et al. RWKV: Reinventing RNNs for the transformer era. In *The 2023 Conference on Empirical Methods in Natural Language Processing*, 2023.

Aleksandar Petrov, Philip HS Torr, and Adel Bibi. When do prompting and prefix-tuning work? a theory of capabilities and limitations. In *International Conference on Learning Representations*, 2024.

Torsten Scholak, Nathan Schucher, and Dzmitry Bahdanau. PICARD: Parsing incrementally for constrained auto-regressive decoding from language models. In *Proceedings of the 2021 Conference on Empirical Methods in Natural Language Processing*, pp. 9895–9901, 2021.

Weixi Song, Zuchao Li, Lefei Zhang, Hai Zhao, and Bo Du. Sparse is enough in fine-tuning pre-trained large language model. *arXiv preprint arXiv:2312.11875*, 2023.

Yutao Sun, Li Dong, Shaohan Huang, Shuming Ma, Yuqing Xia, Jilong Xue, Jianyong Wang, and Furu Wei. Retentive network: A successor to transformer for large language models. *arXiv preprint arXiv:2307.08621*, 2023.

Ashish Vaswani, Noam Shazeer, Niki Parmar, Jakob Uszkoreit, Llion Jones, Aidan N Gomez, Łukasz Kaiser, and Illia Polosukhin. Attention is all you need. In *Advances in Neural Information Processing Systems*, volume 30, 2017.

Alex Wang, Amanpreet Singh, Julian Michael, Felix Hill, Omer Levy, and Samuel R. Bowman. GLUE: A multi-task benchmark and analysis platform for natural language understanding. In *International Conference on Learning Representations*, 2019.

Hongyi Wang, Saurabh Agarwal, and Dimitris Papailiopoulos. Pufferfish: Communication-efficient models at no extra cost. In *Proceedings of Machine Learning and Systems*, volume 3, pp. 365–386, 2021.

Hongyi Wang, Saurabh Agarwal, Yoshiki Tanaka, Eric Xing, Dimitris Papailiopoulos, et al. Cuttlefish: Low-rank model training without all the tuning. *Proceedings of Machine Learning and Systems*, 5, 2023a.

Yihan Wang, Jatin Chauhan, Wei Wang, and Cho-Jui Hsieh. Universality and limitations of prompt tuning. In *Advances in Neural Information Processing Systems*, 2023b.

Masakazu Yoshimura, Teruaki Hayashi, and Yota Maeda. Mambapeft: Exploring parameter-efficient fine-tuning for mamba. *arXiv preprint arXiv:2411.03855*, 2024.

Tao Yu, Rui Zhang, Kai Yang, Michihiro Yasunaga, Dongxu Wang, Zifan Li, James Ma, Irene Li, Qingning Yao, Shanelle Roman, et al. Spider: A large-scale human-labeled dataset for complex and cross-domain semantic parsing and text-to-sql task. In *Proceedings of the 2018 Conference on Empirical Methods in Natural Language Processing*, pp. 3911–3921, 2018.

Elad Ben Zaken, Yoav Goldberg, and Shauli Ravfogel. BitFit: Simple parameter-efficient fine-tuning for transformer-based masked language-models. In *Proceedings of the 60th Annual Meeting of the Association for Computational Linguistics (Volume 2: Short Papers)*, pp. 1–9, 2022.

Yuchen Zeng and Kangwook Lee. The expressive power of low-rank adaptation. In *International Conference on Learning Representations*, 2024.

Appendix

| | |
|---------------------------------------------------------------------------------|-----------|
| A Extended Related Works | 16 |
| A.1 Extended Related Works on SSMs | 16 |
| A.2 Extended Related Works on PEFT | 16 |
| B Details of Datasets | 17 |
| C Details of Sec. 4: Benchmarking PEFT Methods on SSM-based Models | 18 |
| C.1 Experiment Setup | 18 |
| C.2 Extended Results on Benchmarking Existing PEFT Methods | 18 |
| C.3 Limitations of Applying Input-injected Methods on SSMs | 19 |
| C.4 Optimal Application of LoRA* in SSM-based Models | 25 |
| D Details of Sec. 5: Sparse Dimension Tuning | 26 |
| D.1 Details of Sec. 5.1: Understanding Key Parameters in S4 Modules | 26 |
| D.2 Details of Sec. 5.2: Sparse Dimension Tuning and Pruning (SDT-P) | 28 |
| D.3 Details of Sec. 5.3: Expressive Power of SDT-P Combined with LoRA | 29 |
| D.3.1 Extending the Analysis to Deep S4 Models | 29 |
| D.3.2 Extending the Analysis to S6 | 31 |
| D.4 Details of Sec. 5.4: Sparse Dimension Tuning | 32 |
| E Expanded Sec. 6: Evaluation of SDT | 34 |
| E.1 Experiments on Deep S4 Models | 34 |
| E.2 Experiments on Mamba-I, Mamba-II, and Jamba | 34 |

A Extended Related Works

A.1 Extended Related Works on SSMs

Linear State-Space Layers (LSSL) represent one of the earliest SSM layers utilized in deep learning, functioning as continuous-time, recurrent, and convolutional models (Gu et al., 2021). LSSL employs HiPPO theory (Gu et al., 2020) to initialize the state matrix A , enabling the capture of long dependencies. However, LSSL is computationally expensive, limiting its practical application. Gu et al. (2022b) introduced Structured State Space Models (S4), which optimize computation efficiency by employing a structured state matrix A . Gupta et al. (2022) proposed DSS, which simplifies the model by using a diagonal matrix for A and empirically demonstrated that it suffices to achieve performance comparable to S4. Further, Gu et al. (2022a) provided a theoretical explanation for the effectiveness of the diagonal state matrix A in DSS and introduced S4D, which offers various initialization methods for A . Subsequently, the diagonal structure of the state matrix A has been adopted in follow-up methods (Gu & Dao, 2024). Despite differences in optimization algorithms, we refer to S4 and its close variants, including DSS and S4D, collectively as S4. This terminology encompasses models that maintain the standard discrete-time SSM form with a diagonal state matrix.

Despite of the remarkable performance of SSMs on certain tasks of sequence modeling, SSMs still showed worse performance than Transformers on language modeling. Fu et al. (2022) transitioned from synthetic language modeling tasks to real language modeling tasks with SSMs. They proposed H3, which is inspired by Linear Attention (Katharopoulos et al., 2020), introducing both diagonal SSM and shift SSM. Recently, Mamba (Gu & Dao, 2024; Dao & Gu, 2024) escaped from linear time invariance (LTI) modeling by introducing input-dependent terms and achieved better performance than Transformer on language modeling. Furthermore, several hybrid models (Lieber et al., 2024; Park et al., 2024) tried to exploit the advantages of both SSMs and Transformers.

A.2 Extended Related Works on PEFT

In this section, we provide a more detailed description of the baseline methods.

LoRA (Hu et al., 2021). LoRA (Low-Rank Adaptation) focuses on fine-tuning large models by freezing most of the pretrained parameters and injecting trainable low-rank matrices into each layer of the Transformer’s architecture. The intuition behind using low-rank matrices comes from linear algebra, where a large matrix can be closely approximated by the product of two smaller matrices. The number of trainable parameters can be controlled with the rank of the low-rank matrices. LoRA also uses a scaling parameter (LoRA alpha) for the weight matrices to control the balance of the original model weights and LoRA weights during training. After fine-tuning, LoRA weights can be merged with the original model weights, introducing no additional inference overhead.

Prompt Tuning (Lester et al., 2021). Prompt tuning freezes all model weights and prepends a trainable soft prompt to the input prompt. The soft prompt consists of trainable virtual tokens, which are continuous. At inference time, prompt tuning introduces an inference overhead based on the number of virtual tokens used.

Prefix-Tuning (Li & Liang, 2021). Prefix-tuning also prepends trainable tokens to the input like prompt tuning but injects separate prefixes in every layer. For each Transformer layer, prefix-tuning prepends trainable embeddings to the attention’s K and V matrix. The authors have found that directly training these prefixes can lead to unstable training, so they propose to over-parameterize them with a large MLP to increase training stability. After training, the MLP can be dropped. Like prompt tuning, prefix-tuning introduces an inference overhead, scaling linearly with the number of trainable embeddings.

BitFit (Zaken et al., 2022). BitFit is a simple but effective PEFT method that freezes all model weights except the bias terms, consequently greatly reducing the number of trainable parameters. As no additional parameters are added, no inference overhead occurs.

Theoretical understanding of PEFT. Numerous efforts have been made to theoretically understand existing PEFT methods. For input-injected methods, Wang et al. (2023b), Petrov et al. (2024), and

Oymak et al. (2023) have theoretically analyzed the effectiveness and limitations of prompt tuning and prefix-tuning for Transformer-based models. For LoRA, Zeng & Lee (2024) explored its expressive power by demonstrating that even a randomly initialized model can be adapted to match any smaller target model using LoRA. Some of our theoretical analysis draws upon the framework established by Zeng & Lee (2024). Jang et al. (2024) conducted a theoretical exploration of LoRA within the neural tangent kernel (NTK) regime.

B Details of Datasets

In this paper, we consider five datasets across three domains: (i) Natural Language Understanding (NLU), represented by GLUE (Wang et al., 2019); (ii) Natural Language Generation (NLG), including SAMSum (Gliwa et al., 2019), Spider (Yu et al., 2018) and DART (Nan et al., 2021); and (iii) Computer Vision (CV), represented by CIFAR-10 (Krizhevsky et al., 2009).

GLUE (Wang et al., 2019). The GLUE (General Language Understanding Evaluation) benchmark is a collection of datasets used for training, evaluating, and analyzing natural language understanding models across a range of diverse tasks. The benchmark includes nine sentence- or sentence-pair language understanding tasks that require various features of understanding, such as sentiment analysis, linguistic acceptability, semantic textual similarity, and question answering. We use seven datasets from the GLUE benchmark (RTE, MRPC, CoLA, SST-2, QNLI, QQP, MNLI) where the model has to choose between two or three (for MNLI) different choices for the respective task. Except for CoLA, we evaluate all used datasets with the accuracy metric. For CoLA, Matthews correlation is employed.

SAMSum (Gliwa et al., 2019). SAMSum is a dataset for dialogue summarization research, comprising approximately 16,000 synthetic text conversations with accompanying summaries. Created by English-fluent linguists, these exchanges simulate real-world digital communications across various topics and styles. The conversations range from informal to formal, incorporating elements like slang and emoticons to reflect authentic messaging patterns. Each dialogue is paired with a concise, third-person summary, capturing its essential content. This structure makes SAMSum particularly useful for developing and evaluating automated summarization systems capable of processing conversational text.

Spider (Yu et al., 2018). Spider is a large-scale, complex, and cross-domain semantic parsing and text-to-SQL dataset. It contains about 10,000 annotated SQL queries, distributed across 200+ databases, each with multiple tables. We follow Scholak et al. (2021) and use about 7,000 examples for training and about 1,000 examples for validation, where we ignore sequences longer than 1536 tokens. The dataset consists of English question and SQL query pairs, which cover a wide range of SQL operations including SELECT, WHERE, COUNT, GROUP BY, ORDER BY, JOIN, and more. Given an English question and an SQL database scheme, the task for the model is to translate the English question into an appropriate SQL statement. Evaluation is performed via accuracy where the output is considered as correct if the model’s predicted SQL query and the included GT SQL query give the same result when executed on the database. The dataset additionally categorizes each query into easy (25%), medium (40%), hard (20%), and extra hard (15%) based on the complexity of the required SQL statement. For evaluation, we report the execution accuracy of all categories.

DART (Nan et al., 2021). The DART (DAta Record to Text) benchmark is a large-scale, structured dataset designed for RDF-to-text (Resource Description Framework-to-text) generation with 80,000+ instances. The DART benchmark is composed of a collection of structured data triples and corresponding text summaries which are organized into different categories. The task of the DART benchmark is to generate natural language summaries that correctly represent the given structured data inputs. DART is typically evaluated with METEOR and BLEU.

CIFAR-10 (Krizhevsky et al., 2009). The CIFAR-10 (Canadian Institute For Advanced Research) dataset is a collection of images that are commonly used to train machine learning and computer vision algorithms. It is one of the most widely used datasets for image classification. The CIFAR-10 dataset contains 60,000 (50,000 for training, 10,000 for validation) 32×32 color images in 10 different classes. The 10 different classes are: airplane, car, bird, cat, deer, dog, frog, horse, ship, and truck.

| Dataset | Size (Train) | Size (Val) | Size (Test) | Max. seq. len. | #Epochs | Mamba Size | Jamba Size | Metrics | |
|----------|--------------|------------|-------------|----------------|---------|------------|------------|---------|----------------|
| GLUE | RTE | 1992 | 498 | 277 | 291 | 10 | 130M | 319M | Accuracy |
| | MRPC | 2934 | 734 | 408 | 105 | 10 | 130M | 319M | Accuracy |
| | CoLA | 6840 | 1711 | 1043 | 47 | 10 | 130M | 319M | Matthews corr. |
| | SST-2 | 53879 | 13470 | 872 | 68 | 10 | 130M | 319M | Accuracy |
| | QNLI | 83794 | 20949 | 5463 | 602 | 10 | 130M | 319M | Accuracy |
| | QQP | 291076 | 72770 | 40430 | 316 | 3 | 130M | 319M | Accuracy |
| | MNLI | 314161 | 78541 | 19647 | 425 | 3 | 130M | 319M | Accuracy |
| | Spider | 5543 | 1375 | 1034 | 1412 | 10 | 1.4B, 2.8B | 52B | Accuracy |
| | SAMSum | 14732 | 818 | 819 | 1174 | 10 | 1.4B | 52B | ROUGE |
| | DART | 62659 | 2768 | 5097 | 491 | 10 | 130M | 52B | METEOR, BLEU |
| CIFAR-10 | CIFAR-10 | 40000 | 10000 | 10000 | 1730 | 5 | 130M | 319M | Accuracy |
| | CelebA | 162770 | 19867 | 19962 | 12614 | 3 | 130M | 319M | Accuracy |

Table 5: **Datasets and models for our experiments.** For each dataset, we report the number of training, validation, and test samples, maximum sequence length, training epochs, model size, and evaluation metric used.

There are 6,000 images of each class. For training, we center crop each image to 24×24 pixels and flatten each image to a string, with a total of $24 \times 24 \times 3$ words, where each word is a number between 0-255 representing the respective pixel value. Although CIFAR-10 is a dataset for computer vision, previous work (Dinh et al., 2022) showed that Transformers can be adapted to the vision domain from the language domain, and we tested this ability on the state-space model.

CelebA (Liu et al., 2015). The CelebA (CelebFaces Attributes) dataset is an extensive collection of more than 200,000 celebrity images, each tagged with 40 attributes. This dataset is notable for its diversity, volume, and comprehensive annotations, encompassing 10,177 distinct identities, 202,599 facial images, and annotations of five landmark points with 40 binary attributes per image. The dataset, which includes images with varied poses and complex backgrounds, is an essential resource for tasks in computer vision such as face recognition, attribute analysis, and detection, as well as facial landmark localization, and it offers significant utility in face editing and synthesis.

The dataset characteristics, including our train, validation and test set sizes, sequence lengths, and number of epochs, are summarized in Table 5.

C Details of Sec. 4: Benchmarking PEFT Methods on SSM-based Models

In this section, we provide a comprehensive experimental setup, proofs and further discussion of theoretical results, and additional experiment results.

C.1 Experiment Setup

For each dataset, we choose the model size depending on how challenging the dataset is and perform a small grid search for one epoch on a subset of the data (1k-2k instances) with learning rates $\{4 \times 10^{-1}, 2 \times 10^{-1}, 1 \times 10^{-1}, \dots, 1 \times 10^{-5}\}$ to find the optimal learning rate of each PEFT method. We only report the validation metric of the best epoch during training (early stopping) in our results. We fine-tune pretrained Mamba and Jamba models with AdamW with a linear learning rate decay schedule. For LoRA we set rank to 8, alpha to 8, and dropout to 0.1 for all experiments. For evaluating NLG tasks, we employ beam search with five beams and a maximum beam length of 1024.

C.2 Extended Results on Benchmarking Existing PEFT Methods

Mamba-I. We present comprehensive fine-tuning results for the GLUE benchmark (Wang et al., 2019), DART dataset (Nan et al., 2021), SAMSum dataset (Gliwa et al., 2019), Spider dataset (Yu et al., 2018), and CIFAR-10 (Krizhevsky et al., 2009) in Table 6, Table 7, Table 8, Table 9, and Table 10 respectively. These experimental results encompass various LoRA implementations (on different weight matrices and modules) and provide more fine-grained results across all subtasks.

As shown in all these tables, the performance of applying LoRA to $\mathbf{W}_{\text{in},x}$, $\mathbf{W}_{\text{in},z}$, \mathbf{W}_{out} is quite similar across different datasets, with no consistent trend—one occasionally outperforming the others. Therefore, in Sec. 4, we report results only for $\mathbf{W}_{\text{in},x}$ and $\mathbf{W}_{\text{in},z}$.

Mamba-II. Table 11 and Table 12 present the benchmark results of LoRA and full fine-tuning across different layers of Mamba-II. We follow the same experimental setup used for Mamba-I and demonstrate that, on Mamba-II, our conclusion holds: LoRA is more effective on linear projection layers than on SSM modules.

Jamba. Table 13 presents the benchmark results of LoRA and full fine-tuning across different layers of Jamba. Our findings demonstrate that, on Jamba, LoRA is more effective on linear projection layers than on SSM modules, which aligns with our conclusion on Mamba-I and Mamba-II.

| Layer | Method | # Params (%) | RTE | MRPC | CoLA | SST-2 | QNLI | QQP | MNLI | Avg. |
|----------------------------|---------------------------------------------------------------|------------------|--------|------|------|-------|------|------|------|------|
| Pretrained | | 0.00 | 46.9 | 67.9 | 0.0 | 52.4 | 50.5 | 36.8 | 32.3 | 41.0 |
| All | All | Full | 100.00 | 71.1 | 80.6 | 63.2 | 92.2 | 87.4 | 87.9 | 80.8 |
| | | LoRA | 1.92 | 69.9 | 80.9 | 61.4 | 91.9 | 88.4 | 87.6 | 81.1 |
| Prompt | Prompt Tuning | 16 tokens | 0.01 | 56.0 | 71.6 | 12.0 | 89.4 | 76.8 | 79.6 | 61.5 |
| | Prefix-Tuning | 1 token (no MLP) | 0.03 | 67.5 | 75.7 | 43.4 | 91.5 | 83.4 | 83.1 | 35.6 |
| Bias | β_{Δ} , Conv1d | BitFit | 0.06 | 69.5 | 80.4 | 54.7 | 92.0 | 86.2 | 85.3 | 77.2 |
| | All | LoRA | 1.02 | 70.0 | 82.4 | 57.7 | 93.3 | 88.7 | 88.7 | 82.5 |
| | $\mathbf{W}_{\text{in},x}$ | LoRA | 0.34 | 70.4 | 82.1 | 57.4 | 91.7 | 88.3 | 87.7 | 81.2 |
| Linear Projection Matrices | $\mathbf{W}_{\text{in},z}$ | LoRA | 0.34 | 70.0 | 82.4 | 58.1 | 92.4 | 87.3 | 87.3 | 80.4 |
| | $\mathbf{W}_{\text{in},x}, \mathbf{W}_{\text{in},z}$ | LoRA | 0.68 | 70.4 | 84.3 | 62.4 | 92.5 | 88.6 | 88.3 | 81.7 |
| | \mathbf{W}_{out} | LoRA | 0.34 | 70.4 | 82.8 | 60.6 | 92.4 | 88.4 | 87.7 | 81.5 |
| | All | Full | 4.31 | 69.7 | 78.9 | 59.1 | 91.5 | 88.1 | 87.5 | 80.5 |
| | | LoRA | 0.92 | 66.1 | 78.7 | 57.8 | 90.8 | 87.8 | 86.9 | 79.8 |
| | \mathbf{A} | Full | 0.46 | 68.2 | 82.1 | 54.2 | 90.9 | 86.4 | 87.9 | 79.4 |
| S6 | $\mathbf{W}_B, \mathbf{W}_C, \mathbf{W}_{\Delta, \downarrow}$ | Full | 2.28 | 69.7 | 77.0 | 55.8 | 91.4 | 85.4 | 85.0 | 76.8 |
| | | LoRA | 0.69 | 67.9 | 78.9 | 48.8 | 91.4 | 86.9 | 85.8 | 78.6 |
| | $\mathbf{W}_{\Delta, \uparrow}$ | Full | 1.40 | 66.1 | 75.2 | 56.7 | 91.1 | 86.2 | 87.1 | 78.5 |
| | | LoRA | 0.23 | 67.1 | 79.9 | 55.1 | 90.9 | 52.7 | 86.6 | 78.7 |
| | Conv1d | Full | 0.14 | 68.2 | 78.4 | 57.9 | 91.1 | 86.0 | 86.0 | 78.0 |
| Others | $D, \text{LayerNorm}$ | Full | 0.04 | 65.3 | 79.2 | 40.3 | 91.1 | 83.9 | 86.0 | 67.0 |
| | | | | | | | | | | 73.3 |

Table 6: Full benchmark results on the GLUE (Wang et al., 2019) benchmark using Mamba-I-130M. We report accuracy (\uparrow) for RTE, MRPC, SST-2, QNLI, QQP, and MNLI tasks. CoLA performance is measured using Matthews Correlation Coefficient (\uparrow). In each Mamba block, $\mathbf{W}_{\text{in},x}$ and $\mathbf{W}_{\text{in},z}$ are input projections that preprocess the input for SSM modules and the gating branch, respectively. \mathbf{W}_{out} denotes the output projection after the gating mechanism. \mathbf{W}_B and \mathbf{W}_C are weight matrices for computing input-dependent \mathbf{B}_n and \mathbf{C}_n . $\mathbf{W}_{\Delta, \downarrow}$ and $\mathbf{W}_{\Delta, \uparrow}$ represent down and up projections of low-rank weight matrices in the linear layer computing input-dependent step size Δ_n . β_{Δ} represents the bias in this linear layer. D denotes the weight of residual connections.

C.3 Limitations of Applying Input-injected Methods on SSMs

We start by introducing the necessary notations. Denote the space of S4 mechanisms with D channels as $\mathcal{F}_{S4,D}$. Let $\mathbf{H}_0 = (\mathbf{h}_0^{(1)}, \mathbf{h}_0^{(2)}, \dots, \mathbf{h}_0^{(D)}) \in \mathbb{R}^{H \times D}$ represent the initial hidden state, and $\mathbf{X} = (\mathbf{x}_1, \mathbf{x}_2, \dots, \mathbf{x}_N) \in \mathbb{R}^{D \times N}$ denote the input sequence. The output of the S4 mechanism is represented as $f(\mathbf{X}; \mathbf{H}_0)$. Furthermore, for d -th channel, let state transition matrix $\overline{\mathbf{A}}^{(d)} = \text{diag}(a_1^{(d)}, \dots, a_H^{(d)})$ and input transition vector $\overline{\mathbf{B}}^{(d)} = (b_1, \dots, b_H)^\top$, where $d = 1, \dots, D$. For any vector $\mathbf{v} \in \mathbb{R}^n$, we use $\mathbf{v}_{i:j} \in \mathbb{R}^{j-i}$ to denote the subvector of \mathbf{v} containing elements from $i \in \mathbb{N}^+$ to $j \in \mathbb{N}^+$, where $i < j$. Similarly, for any matrix $\mathbf{M} \in \mathbb{R}^{m \times n}$, we use $\mathbf{M}_{i_1:j_1, i_2:j_2}$ to denote the submatrix containing rows $i_1 \in \mathbb{N}^+$ to $j_1 \in \mathbb{N}^+$ and columns $i_2 \in \mathbb{N}^+$ to $j_2 \in \mathbb{N}^+$, where $i_1 < j_1, i_2 < j_2$.

Proposition 1 (Expressivity of Prefix-Tuning on SSMs). *Let $f \in \mathcal{F}_{S4,D}$ be an S4 mechanism. Consider prefix-tuning that prepends a sequence $\mathbf{P} = (\mathbf{p}_1, \dots, \mathbf{p}_M) \in \mathbb{R}^{D \times M}$ to the input sequence $\mathbf{X} = (\mathbf{x}_1, \mathbf{x}_2, \dots, \mathbf{x}_N) \in \mathbb{R}^{D \times N}$. For any prefix $\mathbf{P} \in \mathbb{R}^{D \times M}$, there exists an initial hidden state $\mathbf{H}_0^* \in \mathbb{R}^{H \times D}$ such that the output of S4 after prefix-tuning and that after initial state tuning are identical, i.e., $f(\mathbf{X}; \mathbf{H}_0^*) \equiv f([\mathbf{P}, \mathbf{X}]; \mathbf{H}_0)_{1:D, M+1:M+N}$ for all $\mathbf{X} \in \mathbb{R}^{D \times N}$.*

| Layer | Method | # Params (%) | METEOR | BLEU |
|--------------------------------|--------------------------------------------------------------|--------------|--------|------|
| All | Full | 100.00 | 71.0 | 51.8 |
| | LoRA | 1.92 | 71.0 | 49.5 |
| | DoRA | 2.02 | 70.9 | 51.4 |
| Prompt | Prompt Tuning | 64 tokens | 0.04 | 66.2 |
| | Prefix-Tuning | 64 tokens | 22.69 | 66.6 |
| Bias | β_{Δ} , Conv1d | BitFit | 0.06 | 67.0 |
| | All | LoRA | 1.02 | 71.2 |
| Linear Projection Matrices | DoRA | 1.09 | 71.2 | 50.8 |
| | $\mathbf{W}_{\text{in},x}$ | LoRA | 0.34 | 70.3 |
| | DoRA | 0.37 | 70.8 | 49.9 |
| $\mathbf{W}_{\text{in},z}$ | LoRA | 0.34 | 70.4 | 49.1 |
| | DoRA | 0.37 | 70.2 | 48.3 |
| | $\mathbf{W}_{\text{in},x}, \mathbf{W}_{\text{in},z}$ | LoRA | 0.68 | 70.9 |
| \mathbf{W}_{out} | DoRA | 0.74 | 70.7 | 51.6 |
| | LoRA | 0.34 | 70.7 | 47.0 |
| | DoRA | 0.36 | 70.7 | 46.0 |
| All | Full | 4.31 | 70.3 | 48.7 |
| | LoRA | 0.92 | 69.9 | 50.8 |
| | DoRA | 0.95 | 70.2 | 50.0 |
| S6 | \mathbf{A} | Full | 0.46 | 69.3 |
| | $\mathbf{W}_B, \mathbf{W}_C, \mathbf{W}_{\Delta,\downarrow}$ | Full | 2.28 | 70.1 |
| | LoRA | 0.69 | 68.8 | 48.0 |
| | DoRA | 0.69 | 68.3 | 47.3 |
| | $\mathbf{W}_{\Delta,\uparrow}$ | Full | 1.40 | 69.6 |
| $\mathbf{W}_{\Delta,\uparrow}$ | LoRA | 0.23 | 68.9 | 47.0 |
| | DoRA | 0.26 | 68.4 | 46.3 |
| Conv1d | Full | 0.14 | 68.6 | 47.9 |
| | $\mathbf{D}, \text{LayerNorm}$ | Full | 0.04 | 67.0 |
| Others | | | | 44.2 |

Table 7: **Full benchmark results on the DART (Nan et al., 2021) benchmark using Mamba-I-130M.** We report METEOR (\uparrow) and BLEU (\uparrow) scores. In each Mamba block, $\mathbf{W}_{\text{in},x}$ and $\mathbf{W}_{\text{in},z}$ are input projections that preprocess the input for SSM modules and the gating branch, respectively. \mathbf{W}_{out} denotes the output projection after the gating mechanism. \mathbf{W}_B and \mathbf{W}_C are weight matrices for computing input-dependent \mathbf{B}_n and \mathbf{C}_n . $\mathbf{W}_{\Delta,\downarrow}$ and $\mathbf{W}_{\Delta,\uparrow}$ represent down and up projections of low-rank weight matrices in the linear layer computing input-dependent step size Δ_n . β_{Δ} represents the bias in this linear layer. \mathbf{D} denotes the weight of residual connections.

Furthermore, assume that $\prod_{0 \leq i < j \leq H} (a_j^{(d)} - a_i^{(d)}) \neq 0$ and $\prod_{k=1}^H b_k^{(d)} \neq 0$ for all channels $d = 1, \dots, D$. Then the converse (i.e., for any $\mathbf{H}_0 \in \mathbb{R}^{H \times D}$, there exists a $\mathbf{P}^* \in \mathbb{R}^{D \times M}$ such that $f([\mathbf{P}^*, \mathbf{X}]; \mathbf{H}_0)_{1:D, M+1:M+N} \equiv f(\mathbf{X}; \mathbf{H}_0^*)$ for all $\mathbf{X} \in \mathbb{R}^{D \times N}$) holds if and only if $M \geq H$.

Proof of Proposition 1. Given that operations in S4 are independent across all channels, we can, without loss of generality, consider the case where the number of channels $D = 1$. Consequently, we can simplify our notation: the initial hidden states $\mathbf{H}_0 \in \mathbb{R}^{H \times D}$ become $\mathbf{h}_0 \in \mathbb{R}^H$, the input sequence $\mathbf{X} \in \mathbb{R}^{D \times N}$ becomes $\mathbf{x} \in \mathbb{R}^N$, and the prefix $\mathbf{P} \in \mathbb{R}^{D \times M}$ becomes $\mathbf{p} \in \mathbb{R}^M$. We omit the superscript (d) denoting the channel index. To differentiate between the hidden states and output of prefix-tuned S4 (i.e., $f([\mathbf{P}, \mathbf{X}]; \mathbf{H}_0)_{1:D, M+1:M+N}$) and initial state tuned S4 (i.e., $f(\mathbf{X}; \mathbf{H}_0^*)$), we introduce superscripts “PT” and “IST” respectively. The “PT” superscript denotes hidden states and output of S4 after prefix-tuning, while “IST” indicates those after initial state tuning.

We divide the proposition into two statements:

1. For any prefix $\mathbf{p} \in \mathbb{R}^M$, there exists an initial hidden state $\mathbf{h}_0^* \in \mathbb{R}^H$ such that the output of S4 after prefix-tuning and that after initial state tuning are identical, i.e., $f(\mathbf{x}; \mathbf{h}_0^*) \equiv f([\mathbf{p}, \mathbf{x}]; \mathbf{h}_0)_{M+1:N+M}$ for all $\mathbf{x} \in \mathbb{R}^N$.
2. Furthermore, assume that $\prod_{0 \leq i < j \leq H} (a_j - a_i) \neq 0$ and $\prod_{k=1}^H b_k \neq 0$. Then the converse (i.e., for any $\mathbf{h}_0 \in \mathbb{R}^H$, there exists a $\mathbf{p}^* \in \mathbb{R}^M$ such that $f([\mathbf{p}^*, \mathbf{x}]; \mathbf{h}_0)_{M+1:N+M} \equiv f(\mathbf{x}; \mathbf{h}_0^*)$ for all $\mathbf{x} \in \mathbb{R}^N$) holds if and only if $M \geq H$.

We will first prove the first statement and then proceed to prove the second statement.

| Layer | Method | # Params (%) | R1 | R2 | RL |
|----------------------------|-----------------------------------|--------------|----------------|--------------|--------------|
| All | All | Full LoRA | 100.00 0.97 | 51.2 50.8 | 27.3 26.6 |
| Prompt | Prompt Tuning | 64 tokens | 0.01 | 50.1 | 25.6 |
| | Prefix-Tuning | 64 tokens | 12.81 | 50.6 | 26.5 |
| Bias | β_{Δ} , Conv1d | BitFit | 0.03 | 50.3 | 25.7 |
| | All | LoRA | 0.51 | 50.8 | 26.9 |
| Linear Projection Matrices | $W_{in,x}$ | LoRA | 0.17 | 49.8 | 25.4 |
| | $W_{in,z}$ | LoRA | 0.17 | 50.0 | 26.1 |
| | $W_{in,x}, W_{in,z}$ | LoRA | 0.34 | 50.9 | 27.0 |
| | W_{out} | LoRA | 0.17 | 49.9 | 25.4 |
| S6 | All | Full LoRA | 4.46 0.46 | 51.1 50.5 | 26.9 26.4 |
| | \mathbf{A} | Full | 0.23 | 50.1 | 25.9 |
| | $W_B, W_C, W_{\Delta,\downarrow}$ | Full LoRA | 2.29 0.35 | 50.5 50.4 | 26.0 26.0 |
| | $W_{\Delta,\uparrow}$ | Full LoRA | 1.85 0.12 | 50.3 50.2 | 25.7 25.4 |
| | Conv1d | Full | 0.07 | 50.1 | 25.7 |
| | $D, \text{LayerNorm}$ | Full | 0.02 | 49.6 | 24.8 |
| | | | | | 41.1 |
| Others | | | | | |

Table 8: **Full benchmark results on the SAMSum (Gliwa et al., 2019) benchmark using Mamba-I-1.4B.** R1, R2, and RL represent ROUGE-1 (\uparrow), ROUGE-2 (\uparrow), and ROUGE-L (\uparrow), respectively. In each Mamba block, $W_{in,x}$ and $W_{in,z}$ are input projections that preprocess the input for SSM modules and the gating branch, respectively. W_{out} denotes the output projection after the gating mechanism. W_B and W_C are weight matrices for computing input-dependent B_n and C_n . $W_{\Delta,\downarrow}$ and $W_{\Delta,\uparrow}$ represent down and up projections of low-rank weight matrices in the linear layer computing input-dependent step size Δ_n . β_{Δ} represents the bias in this linear layer. D denotes the weight of residual connections.

Statement 1. The recurrent computation formulation of S4 in equation 2 implies that for each position i , the output y_i depends solely on the previous hidden state h_{i-1} and the current input x_i . Thus, to demonstrate that $f(\mathbf{x}; \mathbf{h}_0^*) \equiv f([\mathbf{p}, \mathbf{x}]; \mathbf{h}_0)_{M+1:N+M}$ for all $\mathbf{x} \in \mathbb{R}^N$, it suffices to show that the hidden state for predicting output y_1^{IST} equals that for predicting output y_{M+1}^{PT} , where y_1^{IST} and y_{M+1}^{PT} are outputs corresponding to the input x_1 for initial state tuning and prefix-tuning, respectively. In other words, it is sufficient to show that the initial state of initial-state-tuned model $\mathbf{h}_0^{\text{IST}} = \mathbf{h}_0^*$ is equal to the $(M+1)$ -th hidden state of prefix-tuned model $\mathbf{h}_{M+1}^{\text{PT}} = \sum_{m=1}^M \bar{\mathbf{A}}^{M-m} \bar{\mathbf{B}} p_m$. When this equality holds, the subsequent hidden states and outputs for both versions of S4 will be identical, as the input sequence from that point onward is the same. Therefore, We prove the first statement by letting

$$\mathbf{h}_0^* = \sum_{m=1}^M \bar{\mathbf{A}}^{M-m} \bar{\mathbf{B}} p_m.$$

Statement 2. We aim to investigate the conditions under which there exists a $\mathbf{h}_0^* \in \mathbb{R}^H$ such that for any $\mathbf{p} \in \mathbb{R}^M$, $f([\mathbf{p}^*, \mathbf{x}]; \mathbf{h}_0)_{M+1:N+M} \neq f(\mathbf{x}; \mathbf{h}_0^*)$. This is equivalent to demonstrating the existence of $\mathbf{h}_0^* \in \mathbb{R}^H$ such that

$$\mathbf{h}_0^* \neq \sum_{m=1}^M \bar{\mathbf{A}}^{M-m} \bar{\mathbf{B}} p_m, \quad \text{for all } \mathbf{p} \in \mathbb{R}^M.$$

This condition can be further reformulated as

$$\mathbb{R}^H \setminus \text{span}(\bar{\mathbf{A}}^M \bar{\mathbf{B}}, \bar{\mathbf{A}}^{M-1} \bar{\mathbf{B}}, \dots, \bar{\mathbf{B}}) \neq \emptyset,$$

which is equivalent to

$$\text{span}(\bar{\mathbf{A}}^M \bar{\mathbf{B}}, \bar{\mathbf{A}}^{M-1} \bar{\mathbf{B}}, \dots, \bar{\mathbf{B}}) \subsetneq \mathbb{R}^H. \quad (6)$$

| Layer | Method | # Params (%) | All | Easy | Medium | Hard | Extra |
|-----------------------------------|---------------------------|--------------|--------|------|--------|------|-------|
| All | All | Full | 100.00 | 66.2 | 84.3 | 69.5 | 53.4 |
| | | LoRA | 0.97 | 56.4 | 76.2 | 57.0 | 47.7 |
| | | DoRA | 1.02 | 55.7 | 77.0 | 57.0 | 47.1 |
| Prompt | Prompt Tuning | 64 tokens | 0.01 | 43.6 | 65.3 | 42.4 | 33.3 |
| | Prefix-Tuning | 64 tokens | 12.81 | 39.7 | 65.7 | 38.6 | 31.0 |
| Bias | β_{Δ} , Conv1d | BitFit | 0.03 | 51.3 | 74.2 | 50.9 | 43.1 |
| | All | LoRA | 0.51 | 54.7 | 75.0 | 55.6 | 46.0 |
| Linear Projection Matrices | | DoRA | 0.55 | 57.2 | 79.4 | 58.7 | 46.0 |
| | $W_{in,x}$ | LoRA | 0.17 | 60.8 | 76.6 | 63.5 | 52.9 |
| | | DoRA | 0.19 | 58.4 | 80.2 | 60.1 | 49.4 |
| $W_{in,z}$ | LoRA | 0.17 | 46.3 | 68.5 | 45.7 | 36.8 | 24.7 |
| | | DoRA | 0.19 | 59.8 | 83.9 | 60.1 | 50.6 |
| | $W_{in,x}, W_{in,z}$ | LoRA | 0.34 | 57.5 | 77.4 | 58.7 | 45.4 |
| | | DoRA | 0.37 | 60.7 | 78.6 | 62.1 | 52.9 |
| W_{out} | LoRA | 0.17 | 61.8 | 81.9 | 65.2 | 45.4 | 39.8 |
| | | DoRA | 0.18 | 61.3 | 79.4 | 63.9 | 50.0 |
| | All | Full | 4.46 | 56.7 | 76.6 | 57.8 | 46.0 |
| S6 | LoRA | 0.46 | 56.3 | 75.0 | 56.5 | 50.6 | 33.7 |
| | DoRA | 0.48 | 58.9 | 77.4 | 62.1 | 47.1 | 34.9 |
| | A | Full | 0.23 | 51.1 | 71.4 | 52.5 | 42.5 |
| $W_B, W_C, W_{\Delta,\downarrow}$ | Full | 2.29 | 47.2 | 72.2 | 46.9 | 35.6 | 22.9 |
| | LoRA | 0.35 | 55.0 | 73.8 | 56.7 | 44.3 | 33.7 |
| | DoRA | 0.35 | 55.3 | 78.2 | 57.8 | 41.4 | 28.9 |
| $W_{\Delta,\uparrow}$ | Full | 1.85 | 56.8 | 77.0 | 59.4 | 43.7 | 33.1 |
| | LoRA | 0.12 | 58.0 | 78.6 | 59.4 | 48.9 | 33.1 |
| | DoRA | 0.13 | 55.3 | 76.2 | 59.2 | 42.5 | 27.1 |
| Conv1d | Full | 0.07 | 53.2 | 74.6 | 52.9 | 43.7 | 31.9 |
| | D , LayerNorm | Full | 0.02 | 49.6 | 70.6 | 50.4 | 40.2 |
| Others | | | | | | | 25.9 |

(a) Full benchmark results on Spider using Mamba-I 1.4B.

| Layer | Method | # Params (%) | All | Easy | Medium | Hard | Extra |
|----------------------------|-----------------------------------|--------------|--------|------|--------|------|-------|
| All | All | Full | 100.00 | 71.8 | 87.5 | 73.5 | 63.8 |
| | | LoRA | 0.80 | 70.9 | 90.7 | 74.0 | 58.6 |
| Prompt | Prompt Tuning | 64 tokens | 0.01 | 50.7 | 75.4 | 53.8 | 37.4 |
| | Prefix-Tuning | 1 token | 10.82 | 45.1 | 75.0 | 45.1 | 32.2 |
| Bias | β_{Δ} , Conv1d | BitFit | 0.02 | 59.9 | 82.3 | 60.8 | 52.9 |
| | All | LoRA | 0.42 | 58.2 | 74.6 | 58.3 | 51.7 |
| Linear Projection Matrices | $W_{in,x}$ | LoRA | 0.14 | 66.7 | 87.9 | 67.7 | 56.9 |
| | $W_{in,z}$ | LoRA | 0.14 | 65.4 | 86.7 | 68.8 | 54.6 |
| | $W_{in,x}, W_{in,z}$ | LoRA | 0.28 | 65.2 | 89.1 | 67.3 | 51.7 |
| W_{out} | LoRA | 0.14 | 67.0 | 87.1 | 69.1 | 52.9 | 46.4 |
| | All | Full | 4.44 | 65.7 | 81.9 | 68.8 | 58.0 |
| | LoRA | 0.38 | 63.9 | 86.3 | 68.2 | 49.4 | 34.3 |
| A | Full | 0.19 | 56.6 | 77.0 | 58.1 | 46.0 | 33.1 |
| | $W_B, W_C, W_{\Delta,\downarrow}$ | Full | 2.27 | 58.8 | 79.0 | 61.0 | 50.6 |
| S6 | | LoRA | 0.29 | 60.3 | 82.7 | 63.0 | 46.6 |
| | $W_{\Delta,\uparrow}$ | Full | 1.91 | 62.2 | 82.3 | 65.7 | 51.7 |
| Conv1d | LoRA | 0.10 | 62.2 | 80.2 | 66.6 | 49.4 | 36.7 |
| | Full | 0.06 | 62.5 | 81.9 | 66.1 | 51.1 | 35.5 |
| Others | D , LayerNorm | Full | 0.02 | 51.0 | 71.0 | 51.1 | 42.5 |

(b) Full benchmark results on Spider using Mamba-I 2.8B.

Table 9: **Full benchmark results on Spider (Yu et al., 2018) dataset using Mamba-I**. We report the accuracy (\uparrow) for Spider and its subsets. We consider two models in our experiments: Mamba-I 1.4B and Mamba-I 2.8B. In each Mamba block, $W_{in,x}$ and $W_{in,z}$ are input projections that preprocess the input for SSM modules and the gating branch, respectively. W_{out} denotes the output projection after the gating mechanism. W_B and W_C are weight matrices for computing input-dependent B_n and C_n . $W_{\Delta,\downarrow}$ and $W_{\Delta,\uparrow}$ represent down and up projections of low-rank weight matrices in the linear layer computing input-dependent step size Δ_n . β_{Δ} represents the bias in this linear layer. D denotes the weight of residual connections.

| Layer | | Method | # Params (%) | Accuracy |
|----------------------------|------------------------------------|--------|--------------|----------|
| Pretrained | | | 0.00 | 0.08 |
| All | All | Full | 100.00 | 59.96 |
| | | LoRA | 1.92 | 60.35 |
| Bias | β_{Δ} , Conv1d | BitFit | 0.06 | 44.40 |
| | All | LoRA | 1.02 | 62.79 |
| | $W_{\text{in},x}$ | LoRA | 0.34 | 53.49 |
| Linear Projection Matrices | $W_{\text{in},z}$ | LoRA | 0.34 | 58.15 |
| | $W_{\text{in},x}, W_{\text{in},z}$ | LoRA | 0.68 | 61.04 |
| | W_{out} | LoRA | 0.34 | 52.04 |
| | All | Full | 4.31 | 55.51 |
| | | LoRA | 0.92 | 43.96 |
| | A | Full | 0.46 | 61.21 |
| S6 | $W_B, W_C, W_{\Delta,\downarrow}$ | Full | 2.28 | 49.51 |
| | | LoRA | 0.69 | 52.27 |
| | $W_{\Delta,\uparrow}$ | Full | 1.40 | 34.54 |
| | | LoRA | 0.23 | 56.49 |
| | Conv1d | Full | 0.14 | 55.65 |
| Others | D , LayerNorm | Full | 0.04 | 58.09 |

Table 10: **Full benchmark results on the CIFAR-10 (Krizhevsky et al., 2009) dataset using Mamba-I-130M.** We report accuracy (\uparrow). In each Mamba block, $W_{\text{in},x}$ and $W_{\text{in},z}$ are input projections that preprocess the input for SSM modules and the gating branch, respectively. W_{out} denotes the output projection after the gating mechanism. W_B and W_C are weight matrices for computing input-dependent B_n and C_n . $W_{\Delta,\downarrow}$ and $W_{\Delta,\uparrow}$ represent down and up projections of low-rank weight matrices in the linear layer computing input-dependent step size Δ_n . β_{Δ} represents the bias in this linear layer. D denotes the weight of residual connections.

| Layer | | Method | # Params (%) | METEOR | BLEU |
|----------------------------|---------------------------------|--------|--------------|--------|------|
| All | All | Full | 100.00 | 66.6 | 34.9 |
| | | LoRA | 1.39 | 66.9 | 45.4 |
| | $W_{\text{in}}, W_{\text{out}}$ | LoRA | 1.02 | 67.1 | 44.7 |
| Linear Projection Matrices | W_{in} | LoRA | 0.68 | 67.1 | 43.0 |
| | W_{out} | LoRA | 0.34 | 66.8 | 42.3 |
| | All | Full | 4.17 | 65.7 | 39.7 |
| | | LoRA | 0.38 | 64.2 | 40.1 |
| S6 | W_B, W_C, W_{Δ} | Full | 4.00 | 66.0 | 36.2 |
| | | LoRA | 0.38 | 64.8 | 39.5 |

Table 11: **Full benchmark results of LoRA on DART (Nan et al., 2021) dataset using Mamba-II-130M.**

To determine when this condition holds, we analyze three distinct cases: (i) $M < H$, (ii) $M = H$, and (iii) $M > H$.

(*Case 1: When $M < H$*). In this scenario, it is obvious that equation 6 holds. The existence of such a h_0^* is guaranteed because the dimension of the span is at most M , which is strictly less than H . This choice of h_0^* ensures that it cannot be represented as a linear combination of the vectors in the span, thereby establishing the inequality.

| Layer | Method | # Params (%) | All | Easy | Medium | Hard | Extra |
|----------------------------|---------------------------------------------------|--------------|----------------|--------------|--------------|--------------|--------------|
| All | All | Full LoRA | 100.00 0.71 | 64.8 64.5 | 85.9 81.0 | 65.7 66.4 | 54.0 56.9 |
| Linear Projection Matrices | $\mathbf{W}_{\text{in}}, \mathbf{W}_{\text{out}}$ | LoRA | 0.52 | 50.4 | 68.5 | 52.0 | 44.8 |
| | \mathbf{W}_{in} | LoRA | 0.35 | 57.5 | 76.2 | 59.4 | 48.9 |
| | \mathbf{W}_{out} | LoRA | 0.18 | 57.9 | 81.0 | 56.7 | 51.7 |
| S6 | All | Full LoRA | 2.42 0.18 | 55.1 54.1 | 76.2 74.2 | 56.1 58.1 | 42.5 46.0 |
| | \mathbf{A}_{\log} | Full | 0.00 | 21.5 | 46.0 | 18.8 | 11.5 |
| | $\mathbf{W}_B, \mathbf{W}_C, \mathbf{W}_\Delta$ | Full LoRA | 2.34 0.18 | 50.3 55.5 | 73.0 77.4 | 52.2 55.2 | 39.7 46.6 |

Table 12: Full benchmark results on the Spider (Yu et al., 2018) dataset using Mamba-II 1.3B.

| Layer | Method | # Params (%) | METEOR | BLEU |
|---------------------------------|-------------------------------------------------|--------------|--------|------|
| All | All | Full | 100.00 | 70.8 |
| Attention | All | LoRA | 0.02 | 63.5 |
| MLP | All | LoRA | 1.37 | 70.9 |
| Linear Projection Matrices + S6 | All | LoRA | 0.31 | 70.2 |
| Linear Projection Matrices | \mathbf{W}_{in} | LoRA | 0.11 | 68.9 |
| | \mathbf{W}_{out} | LoRA | 0.05 | 67.7 |
| S6 | All | Full | 0.54 | 69.2 |
| | $\mathbf{W}_B, \mathbf{W}_C, \mathbf{W}_\Delta$ | LoRA | 0.15 | 66.6 |

Table 13: Full benchmark results on DART (Nan et al., 2021) dataset using Jamba-Tiny-319M.

(Case 2: When $M = H$). In this scenario, $\text{span}(\overline{\mathbf{A}}^M \overline{\mathbf{B}}, \overline{\mathbf{A}}^{M-1} \overline{\mathbf{B}}, \dots, \overline{\mathbf{B}}) = \mathbb{R}^H$ if and only if $(\overline{\mathbf{A}}^M \overline{\mathbf{B}}, \overline{\mathbf{A}}^{M-1} \overline{\mathbf{B}}, \dots, \overline{\mathbf{B}})$ are linearly independent. Note that

$$\det(\overline{\mathbf{A}}^M \overline{\mathbf{B}}, \overline{\mathbf{A}}^{M-1} \overline{\mathbf{B}}, \dots, \overline{\mathbf{B}}) = \det(\overline{\mathbf{A}}^M, \overline{\mathbf{A}}^{M-1}, \dots, \mathbf{1}) \prod_{k=1}^H b_k, \quad (7)$$

where

$$\begin{aligned} \det(\overline{\mathbf{A}}^M, \overline{\mathbf{A}}^{M-1}, \dots, \mathbf{1}) &= \det \begin{bmatrix} a_1^{H-1} & \dots & a_1^2 & a_1 & 1 \\ a_2^{H-1} & \dots & a_2^2 & a_2 & 1 \\ \vdots & \ddots & \vdots & \vdots & \vdots \\ a_H^{H-1} & \dots & a_H^2 & a_H & 1 \end{bmatrix} && \text{(Expand)} \\ &= (-1)^{\frac{H(H-1)}{2}} \prod_{0 \leq i < j \leq H} (a_j - a_i). && \text{(Vandermonde matrix)} \quad (8) \end{aligned}$$

| Task | RTE | MRPC | CoLA | SST-2 | QNLI | QQP | MNLI | Avg. Score |
|-----------------------------------|-------------|-------------|-------------|-------------|-------------|-------------|-------------|-------------|
| Prompt Tuning | 56.0 | 71.6 | 12.0 | 89.4 | 76.8 | 79.6 | 61.5 | 63.8 |
| Prefix-Tuning | <u>69.5</u> | <u>75.7</u> | 43.4 | 91.5 | 83.4 | 83.1 | 35.6 | 68.6 |
| Initial State Tuning | 66.8 | 75.1 | <u>52.4</u> | <u>92.4</u> | <u>86.4</u> | <u>86.1</u> | <u>78.5</u> | <u>76.8</u> |
| LoRA (Linear Projection Matrices) | 70.4 | 82.8 | 60.6 | 92.4 | 88.4 | 87.7 | 81.5 | 80.5 |

Table 14: Comparison of prompt-tuning, prefix-tuning, initial state tuning, and LoRA on seven tasks from the GLUE benchmark. We report the Matthews correlation (\uparrow) for CoLA, overall (matched and mismatched) accuracy (\uparrow) for MNLI, and accuracy for other tasks. Initial State Tuning and LoRA are constrained to use less than 0.5% trainable parameters. **Bold** numbers indicate the best performance across all three methods, while underlined numbers show the highest score among input-injected methods (prefix-tuning and initial state tuning). Initial state tuning outperforms prefix-tuning and prompt-tuning on five out of seven tasks, while LoRA consistently outperforms all input-injected methods.

Combining equation 7 and equation 8 yields

$$\det(\bar{\mathbf{A}}^M \bar{\mathbf{B}}, \bar{\mathbf{A}}^{M-1} \bar{\mathbf{B}}, \dots, \bar{\mathbf{B}}) = (-1)^{\frac{H(H-1)}{2}} \prod_{0 \leq i < j \leq H} (a_j - a_i) \prod_{k=1}^H b_k.$$

Therefore, if and only if $\prod_{0 \leq i < j \leq H} (a_j - a_i) \neq 0$ and $\prod_{k=1}^H b_k \neq 0$, we have

$$\det(\bar{\mathbf{A}}^M \bar{\mathbf{B}}, \bar{\mathbf{A}}^{M-1} \bar{\mathbf{B}}, \dots, \bar{\mathbf{B}}) \neq 0,$$

which is both necessary and sufficient for the linear independence of $(\bar{\mathbf{A}}^M \bar{\mathbf{B}}, \bar{\mathbf{A}}^{M-1} \bar{\mathbf{B}}, \dots, \bar{\mathbf{B}})$, and consequently, for the condition in equation 6 to be satisfied.

(Case 3: When $M > H$). The analysis presented in case 2 extends naturally to this scenario.

The combination of the three cases above completes the proof of statement 2. \square

C.4 Optimal Application of LoRA* in SSM-based Models

Several studies (Hu et al., 2023; He et al., 2021) present findings on Transformers, indicating that applying LoRA* to linear projection matrices yields performance comparable to that of sequence-to-sequence modules (i.e., attention layers in Transformers). In contrast, our experimental results on SSMs reveal that applying LoRA* to linear projection matrices is more effective than applying it to sequence-to-sequence modules (i.e., S6 in Mamba-I). Lemma 1 in the main body offers insights into this phenomenon. Here, we provide a more in-depth discussion by presenting its formal version along with its proof.

Notations. For the feasibility of the analysis, we consider a simplified SSM-based architecture which only consists of the input projection matrix $\mathbf{W}_{\text{in}} \in \mathbb{R}^{D \times D}$ and the S6 module parameterized by diagonal state transition matrices $\{\mathbf{A}^{(d)}\}_{d=1}^D$ with $\mathbf{A}^{(d)} \in \mathbb{R}^{H \times H}$, the weight matrices $\mathbf{W}_B, \mathbf{W}_C \in \mathbb{R}^{H \times D}$ for computing input-dependent input transition vectors $\mathbf{B}_n \in \mathbb{R}^H$ and output mapping vectors $\mathbf{C}_n \in \mathbb{R}^H$, the down and up projection matrices $\mathbf{W}_{\Delta, \downarrow} \in \mathbb{R}^{D \times R}, \mathbf{W}_{\Delta, \uparrow} \in \mathbb{R}^{R \times D}$ (where R is the rank) for low-rank weight matrices for computing the input-dependent step size $\Delta_n = (\Delta_n^{(1)}, \dots, \Delta_n^{(D)}) \in \mathbb{R}_D$, for $n = 1, \dots, N$. Define $\mathbf{W}_{\text{S6}} = [\mathbf{W}_B^\top, \mathbf{W}_C^\top, \mathbf{W}_{\Delta, \uparrow}^\top]^\top \in \mathbb{R}^{(2H+R) \times D}$. In the Mamba implementation, \mathbf{W}_{S6} is implemented as the weight matrix of a single linear layer, referred to as `x_proj` in the codebase. Therefore, the parameters of the S6 can be formulated as

$$\theta(\cdot; \{\mathbf{A}\}_{d=1}^D, \mathbf{W}_{\text{S6}}, \mathbf{W}_{\Delta, \downarrow}, \mathbf{W}_{\text{in}}) = \{\bar{\mathbf{A}}_n, \bar{\mathbf{B}}_n, \mathbf{C}_n\}_{n=1}^N.$$

Consider input sequence $\mathbf{X} = (\mathbf{x}_1, \dots, \mathbf{x}_N) \in \mathbb{R}^{D \times N}$. Let $\mathbf{Z} = (\mathbf{z}_1, \dots, \mathbf{z}_N) \in \mathbb{R}^{D \times N}$ denote the intermediate output after the input projection. The intermediate output at position $n \in \{1, \dots, N\}$ is

$$\mathbf{z}_n = \mathbf{W}_{\text{in}} \mathbf{x}_n. \quad (9)$$

Note that

$$\mathbf{B}_n = \mathbf{W}_B \mathbf{z}_n, \quad \mathbf{C}_n = \mathbf{W}_C \mathbf{z}_n, \quad \Delta_n = \text{softplus}(\mathbf{W}_{\Delta, \uparrow} \mathbf{W}_{\Delta, \downarrow} \mathbf{z}_n + \beta_\Delta), \quad (10)$$

and after discretization, we have

$$\bar{\mathbf{A}}_n^{(d)} = \exp(\Delta_n^{(d)} \mathbf{A}^{(d)}), \quad \bar{\mathbf{B}}_n = \Delta_n^{(d)} \mathbf{B}_n = \Delta_n^{(d)} \mathbf{W}_B \mathbf{z}_n. \quad (11)$$

Combining equation 9, equation 10 and equation 11 yields

$$\begin{aligned} \theta(\mathbf{X}; \{\mathbf{A}\}_{d=1}^D, \mathbf{W}_{\text{S6}}, \mathbf{W}_{\Delta, \downarrow}, \mathbf{W}_{\text{in}}) &= \{\bar{\mathbf{A}}_n, \bar{\mathbf{B}}_n, \mathbf{C}_n\}_{n=1}^N, \text{ where} \\ \bar{\mathbf{A}}_n^{(d)} &= \exp(\Delta_n^{(d)} \mathbf{A}^{(d)}), \quad \bar{\mathbf{B}}_n^{(d)} = \Delta_n^{(d)} \mathbf{W}_B \mathbf{W}_{\text{in}} \mathbf{x}_n, \quad \mathbf{C}_n = \mathbf{W}_C \mathbf{W}_{\text{in}} \mathbf{x}_n, \\ \Delta_n &= \text{softplus}(\mathbf{W}_{\Delta, \downarrow} \mathbf{W}_{\Delta, \uparrow} \mathbf{W}_{\text{in}} \mathbf{x}_n + \beta_\Delta). \end{aligned} \quad (12)$$

Theoretical Analysis. In the following theorem, we demonstrate that applying LoRA* exclusively to \mathbf{W}_{in} is equivalent to applying it to \mathbf{W}_{S6} .

Lemma 3 (Detailed Version of Lemma 1). *Consider a model consists of an S6 module augmented with a linear input projection $\mathbf{W}_{\text{in}} \in \mathbb{R}^{D \times D}$. For any fine-tuned model where only \mathbf{W}_{S6} is updated to $\widehat{\mathbf{W}}_{\text{S6}}$, there exists $\widehat{\mathbf{W}}_{\text{in}}$ such that updating only \mathbf{W}_{in} to $\widehat{\mathbf{W}}_{\text{in}}$ yields:*

$$\theta(\mathbf{X}; \{\mathbf{A}^{(d)}\}_{d=1}^D, \overline{\mathbf{W}}_{\text{S6}}, \mathbf{W}_{\Delta, \downarrow}, \mathbf{W}_{\text{in}}) = \theta(\mathbf{X}; \{\mathbf{A}^{(d)}\}_{d=1}^D, \mathbf{W}_{\text{S6}}, \mathbf{W}_{\Delta, \downarrow}, \widehat{\mathbf{W}}_{\text{in}}) \quad (13)$$

Proof of Lemma 3. In this proof, we use $\overline{\cdot}$ to denote the corresponding notations for the model with only \mathbf{W}_{S6} updated, and use $\widehat{\cdot}$ to denote the corresponding notations for the model with only \mathbf{W}_{in} updated. To demonstrate equation 13, it is sufficient, according to equation 12, to find $\widehat{\mathbf{W}}_{\text{in}}$ that satisfies the following equations:

$$\begin{aligned} \overline{\mathbf{W}}_C \mathbf{W}_{\text{in}} &= \mathbf{W}_C \widehat{\mathbf{W}}_{\text{in}} \\ \overline{\mathbf{W}}_{\Delta, \uparrow} \mathbf{W}_{\text{in}} &= \mathbf{W}_{\Delta, \uparrow} \widehat{\mathbf{W}}_{\text{in}} \\ \overline{\mathbf{W}}_B \mathbf{W}_{\text{in}} &= \mathbf{W}_B \widehat{\mathbf{W}}_{\text{in}}. \end{aligned} \quad (14)$$

Since $\mathbf{W}_{\text{S6}} = \begin{bmatrix} \mathbf{W}_B \\ \mathbf{W}_C \\ \mathbf{W}_{\Delta, \uparrow} \end{bmatrix}$, the three conditions equation 14 can be written as

$$\overline{\mathbf{W}}_{\text{S6}} \mathbf{W}_{\text{in}} = \mathbf{W}_{\text{S6}} \widehat{\mathbf{W}}_{\text{in}}. \quad (15)$$

By applying Singular Value Decomposition (SVD) to \mathbf{W}_{S6} and $(\mathbf{W}_{\text{S6}} - \overline{\mathbf{W}}_{\text{S6}}) \mathbf{W}_{\text{in}}$, we obtain:

$$\begin{aligned} \mathbf{W}_{\text{S6}} &= \mathbf{U} [\Sigma \ O_{(2H+R) \times (D-2H-R)}] \mathbf{V}^\top, \\ (\mathbf{W}_{\text{S6}} - \overline{\mathbf{W}}_{\text{S6}}) \mathbf{W}_{\text{in}} &= \mathbf{U}' [\Sigma' \ O_{(2H+R) \times (D-2H-R)}] \mathbf{V}'^\top, \end{aligned} \quad (16)$$

where $\mathbf{U}, \mathbf{U}' \in \mathbb{R}^{(2H+R) \times (2H+R)}$, $\Sigma, \Sigma' \in \mathbb{R}^{(2H+R) \times (2H+R)}$, and $\mathbf{V}, \mathbf{V}' \in \mathbb{R}^{D \times D}$. The diagonal elements of Σ and Σ' are in decreasing order.

We let

$$\widehat{\mathbf{W}}_{\text{in}} = \mathbf{V} \begin{bmatrix} \Sigma^{-1} \mathbf{U}^\top \overline{\mathbf{W}}_{\text{S6}} \mathbf{W}_{\text{in}} \\ \mathbf{Q} \end{bmatrix}, \quad (17)$$

where $\mathbf{Q} \in \mathbb{R}^{(D-2H-R) \times D}$ is an arbitrary matrix to be determined later. Plugging equation 16 and equation 17 back to $\mathbf{W}_{\text{S6}} \widehat{\mathbf{W}}_{\text{in}}$ and simplifying results in

$$\begin{aligned} \mathbf{W}_{\text{S6}} \widehat{\mathbf{W}}_{\text{in}} &= \mathbf{U} [\Sigma \ O_{(2H+R) \times (D-2H-R)}] \mathbf{V}^\top \mathbf{V} \begin{bmatrix} \Sigma^{-1} \mathbf{U}^\top \overline{\mathbf{W}}_{\text{S6}} \mathbf{W}_{\text{in}} \\ \mathbf{Q} \end{bmatrix} && \text{(equation 16 \& equation 17)} \\ &= \overline{\mathbf{W}}_{\text{S6}} \mathbf{W}_{\text{in}}, && \text{(Simplifying)} \end{aligned}$$

which demonstrates that equation 15 is satisfied and completes the proof. \square

D Details of Sec. 5: Sparse Dimension Tuning

D.1 Details of Sec. 5.1: Understanding Key Parameters in S4 Modules

Problem Setting. Inspired by Zeng & Lee (2024)’s theoretical analysis of LoRA’s expressive power, we adopt a similar framework to explore the expressive potential of various parameters in the S4 model. Specifically, we assume a target model that performs well on the intended task and a frozen model, which may be either pretrained or randomly initialized. Our goal is to identify a parameter-efficient method to update the frozen model so that it becomes functionally equivalent to the target model. In alignment with Zeng & Lee (2024), we assume that the frozen model’s capacity is equal to or exceeds that of the target model. This assumption is based on two main considerations: (i) analytical tractability, which necessitates that the frozen model must have the potential to match the functionality of the target model, and (ii) a practical rationale, given that the models typically used in practice are often overparameterized. Assume that both the target model and the frozen model are

S4, with the target model having a hidden state dimension H_* and the frozen model having a hidden state dimension $H \geq H_*$. Meanwhile, suppose that all the hidden dimensions of both models are valid, meaning that none of the parameter elements are zero. The target model, frozen model, and the updated model after tuning the parameters on the frozen model can be formulated using discretized parameters $\bar{\mathbf{A}}, \bar{\mathbf{B}}, \mathbf{C}$ as follows:

$$\begin{aligned}
 \text{(Target model)} \quad f^*(\mathbf{x})_n &= \sum_{m=1}^n \mathbf{C}_* \bar{\mathbf{A}}_*^{m-n} \bar{\mathbf{B}}_* x_m, \text{ where } \text{diag}(\bar{\mathbf{A}}_*) \in \mathbb{R}^{H_*}, \\
 \text{(Frozen model)} \quad f_0(\mathbf{x})_n &= \sum_{m=1}^n \mathbf{C} \bar{\mathbf{A}}^{m-n} \bar{\mathbf{B}} x_m, \text{ where } \text{diag}(\bar{\mathbf{A}}) \in \mathbb{R}^H, \\
 \text{(Updated model)} \quad \hat{f}(\mathbf{x})_n &= \sum_{m=1}^n \hat{\mathbf{C}} \hat{\bar{\mathbf{A}}}^{m-n} \hat{\bar{\mathbf{B}}} x_m, \text{ where } \text{diag}(\hat{\bar{\mathbf{A}}}) \in \mathbb{R}^H.
 \end{aligned}$$

Parameter Efficiency Analysis on S4. Let \mathcal{P}^H denote the set of all $H \times H$ permutation matrices. Given this formulation, we present our first analysis of parameter efficiency for the S4 model in the following lemma. This analysis is based on the parameters after necessary discretization $(\bar{\mathbf{A}}, \bar{\mathbf{B}}, \mathbf{C})$.

Lemma 4 (Essential Discretized Parameter Set for S4). *Consider the parameters after discretization, i.e., $\bar{\mathbf{A}}, \bar{\mathbf{B}}, \mathbf{C}$. To achieve functional equivalence between the updated model and the target model, i.e., $\hat{f} \equiv f^*$, it is sufficient to tune the following number of parameters:*

$$\min_{\mathbf{P} \in \mathcal{P}^H} \underbrace{\left\| [\mathbf{P}^\top (\text{diag}(\bar{\mathbf{A}}) \otimes \bar{\mathbf{B}} \otimes \mathbf{C}^\top)]_{(H_*,+1):H} \right\|_0}_{\text{eliminating redundant dimensions}} + \underbrace{\left\| [\mathbf{P}^\top \bar{\mathbf{A}} \mathbf{P}]_{1:H_*, 1:H_*} - \bar{\mathbf{A}}_* \right\|_0}_{\text{aligning the state matrix}} + \underbrace{\left\| [\mathbf{P}^\top (\bar{\mathbf{B}} \otimes \mathbf{C}^\top)]_{1:H_*} - \bar{\mathbf{B}}_* \otimes \mathbf{C}_*^\top \right\|_0}_{\text{aligning input-output interactions}}.$$

Proof of Lemma 2. The key idea of this proof is straightforward. To facilitate the analysis and update the frozen model to be equivalent to the target model, we first equalize the number of hidden state dimensions between the two models. This is achieved by expanding the target model's \mathbf{A}_* , \mathbf{B}_* , and \mathbf{C}_* to match the H hidden state dimensions of the frozen model, padding the additional $H - H_*$ dimensions with zeros.

Define \otimes as the element-wise product. We can express the target model as:

$$\begin{aligned}
 f^*(\mathbf{x})_n &= \sum_{m=1}^n [\mathbf{C}_* \quad \mathbf{0}^\top] \begin{bmatrix} \bar{\mathbf{A}}_* & \mathbf{O} \\ \mathbf{O} & \mathbf{O} \end{bmatrix}^{n-m} \begin{bmatrix} \bar{\mathbf{B}}_* \\ \mathbf{0} \end{bmatrix} x_m \\
 &= \sum_{m=1}^n \text{diag} \left(\begin{bmatrix} \bar{\mathbf{A}}_* & \mathbf{O} \\ \mathbf{O} & \mathbf{O} \end{bmatrix} \right)^{n-m} \left(\begin{bmatrix} \mathbf{C}_*^\top \\ \mathbf{0} \end{bmatrix} \otimes \begin{bmatrix} \bar{\mathbf{B}}_* \\ \mathbf{0} \end{bmatrix} \right) x_m
 \end{aligned}$$

Consider any permutation matrix $\mathbf{P} \in \mathcal{P}^H$. Applying \mathbf{P} to permute the frozen model leaves the model functionally unchanged:

$$\begin{aligned}
 f_0(\mathbf{x})_n &= \sum_{m=1}^n \mathbf{C} \bar{\mathbf{A}}^{n-m} \bar{\mathbf{B}} x_m = \sum_{m=1}^n \mathbf{C} \mathbf{P} (\mathbf{P}^\top \bar{\mathbf{A}} \mathbf{P})^{n-m} \mathbf{P}^\top \bar{\mathbf{B}} x_m \\
 &= \sum_{m=1}^n \text{diag} (\mathbf{P}^\top \bar{\mathbf{A}} \mathbf{P})^{n-m} ((\mathbf{P}^\top \mathbf{C}^\top) \otimes (\mathbf{P}^\top \bar{\mathbf{B}})) x_m
 \end{aligned}$$

Therefore, to make the updated model equivalent to the target model, we need to update $\mathbf{P}^\top \bar{\mathbf{A}} \mathbf{P}$ to align with $\begin{bmatrix} \bar{\mathbf{A}}_* & \mathbf{O} \\ \mathbf{O} & \mathbf{O} \end{bmatrix}$, and $(\mathbf{P}^\top \mathbf{C}^\top) \otimes (\mathbf{P}^\top \bar{\mathbf{B}})$ to align with $\begin{bmatrix} \mathbf{C}_*^\top \\ \mathbf{0} \end{bmatrix} \otimes \begin{bmatrix} \bar{\mathbf{B}}_* \\ \mathbf{0} \end{bmatrix}$. If they are already matching or partially matched for certain entries, no updates are required for those entries; only the unmatched entries need to be updated. Then, the required trainable parameters for this permutation matrix \mathbf{P} are:

$$\left\| [\mathbf{P}^\top (\text{diag}(\bar{\mathbf{A}}) \otimes \bar{\mathbf{B}} \otimes \mathbf{C}^\top)]_{(H_*,+1):H} \right\|_0 + \left\| [\mathbf{P}^\top \bar{\mathbf{A}} \mathbf{P}]_{1:H_*, 1:H_*} - \bar{\mathbf{A}}_* \right\|_0 + \left\| [\mathbf{P}^\top (\bar{\mathbf{B}} \otimes \mathbf{C}^\top)]_{1:H_*} - \bar{\mathbf{B}}_* \otimes \mathbf{C}_*^\top \right\|_0.$$

Optimizing the permutation matrix $\mathbf{P} \in \mathcal{P}^H$ yields the desired results. \square

This lemma highlights the significance of identifying essential hidden state dimensions. The term $\|[\mathbf{P}^\top(\text{diag}(\overline{\mathbf{A}}) \otimes \overline{\mathbf{B}} \otimes \mathbf{C}^\top)]_{(H_\star+1):H}\|_0$ underscores the importance of excluding redundant dimensions. This can be achieved by either directly removing these dimensions from the state matrix $\overline{\mathbf{A}}$, or by updating $\overline{\mathbf{B}}$ or \mathbf{C} to ensure that only the selected hidden state dimensions are utilized during the input transition or output mapping phases. Once redundant dimensions are filtered out, tuning only the essential dimensions is sufficient to align the updated model with the target model.

Furthermore, based on the lemma, the roles of the input transition vector $\overline{\mathbf{B}}$ and \mathbf{C}^\top are nearly identical, as they consistently appear together as the combined term $\overline{\mathbf{B}} \otimes \mathbf{C}^\top$, which is also discussed in [Gupta et al. \(2022\)](#). Consequently, one could opt to tune either $\overline{\mathbf{B}}$ or \mathbf{C} exclusively or alternatively, split the indices into two groups, tuning $\overline{\mathbf{B}}$ for the first group and \mathbf{C} for the second. Both vectors indicate how information from different hidden state dimensions is integrated, whereas $\overline{\mathbf{A}}$ plays a distinct role, determining how the hidden states are stored.

In practice, instead of directly using the discretized parameters $\overline{\mathbf{A}}, \overline{\mathbf{B}}, \mathbf{C}$, S4 is implemented using the continuous parameters $\mathbf{A}, \mathbf{B}, \mathbf{C}$ with step size Δ . To provide further practical guidance on parameter tuning, the following two lemmas analyze the parameter efficiency of continuous parameters under different discretization methods: Two exemplary methods of discretization are bilinear and zero-order hold (ZOH):

$$(\text{Bilinear}) \quad \begin{cases} \overline{\mathbf{A}} = (\mathbf{I} - \Delta/2\mathbf{A})^{-1}(\mathbf{I} + \Delta/2\mathbf{A}) \\ \overline{\mathbf{B}} = (\mathbf{I} - \Delta/2\mathbf{A})^{-1} \cdot \Delta\mathbf{B}, \end{cases} \quad (\text{ZOH}) \quad \begin{cases} \overline{\mathbf{A}} = \exp(\Delta\mathbf{A}) \\ \overline{\mathbf{B}} = (\Delta\mathbf{A})^{-1}(\exp(\Delta\mathbf{A}) - \mathbf{I}) \cdot \Delta\mathbf{B}. \end{cases} \quad (18)$$

Lemma 5 (Essential Continuous Parameter Set for S4 with Bilinear Discritization). *Consider the parameters before discretization, i.e., $\mathbf{A}, \mathbf{B}, \mathbf{C}$, and they are discretized via bilinear discretization. To achieve functional equivalence between the updated model and the target model, i.e., $\hat{f} \equiv f^*$, it is sufficient to tune the following number of parameters:*

$$\min_{\mathbf{P} \in \mathcal{P}^H} \underbrace{\|[\Delta\mathbf{P}^\top(\text{diag}(\mathbf{I} + \Delta/2\mathbf{A}) \otimes \mathbf{B} \otimes \mathbf{C}^\top)]_{(H_\star+1):H}\|_0}_{\text{eliminating redundant dimensions}} + \underbrace{\|[\mathbf{P}^\top \mathbf{A} \mathbf{P}]_{1:H_\star, 1:H_\star} - \mathbf{A}_\star\|_0}_{\text{aligning the state matrix}} + \underbrace{\|[\mathbf{P}^\top(\mathbf{B} \otimes \mathbf{C}^\top)]_{1:H_\star} - \mathbf{B}_\star \otimes \mathbf{C}_\star^\top\|_0}_{\text{aligning input-output interactions}}.$$

Proof of Lemma 5. Combining Lemma 2 and the Bilinear discretization method in equation 18 yields the desired results. \square

Lemma 6 (Essential Continuous Parameter Set for S4 with ZOH Discritization). *Consider the parameters before discretization, i.e., $\mathbf{A}, \mathbf{B}, \mathbf{C}$, and they are discretized via ZOH discretization. To achieve functional equivalence between the updated model and the target model, i.e., $\hat{f} \equiv f^*$, it is sufficient to tune the following number of parameters:*

$$\min_{\mathbf{P} \in \mathcal{P}^H} \underbrace{\|[\Delta\mathbf{P}^\top(\text{diag}(\exp(\Delta\mathbf{A}) - \mathbf{I}) \otimes \mathbf{B} \otimes \mathbf{C}^\top)]_{(H_\star+1):H}\|_0}_{\text{eliminating redundant dimensions}} + \underbrace{\|[\mathbf{P}^\top \mathbf{A} \mathbf{P}]_{1:H_\star, 1:H_\star} - \mathbf{A}_\star\|_0}_{\text{aligning the state matrix}} + \underbrace{\|[\mathbf{P}^\top(\mathbf{B} \otimes \mathbf{C}^\top)]_{1:H_\star} - \mathbf{B}_\star \otimes \mathbf{C}_\star^\top\|_0}_{\text{aligning input-output interactions}}.$$

Proof of Lemma 6. Combining Lemma 2 and the ZOH discretization method in equation 18 yields the desired results. \square

The insights provided by Lemma 5 and Lemma 6 are the same as those provided by Lemma 2. The analysis here supports the second step of SDT-P presented in Sec. 5.

D.2 Details of Sec. 5.2: Sparse Dimension Tuning and Pruning (SDT-P)

Alg. 2 presents the pseudocode for SDT-P, which includes setting certain dimensions to zero. However, in practice, setting channels to zero is unnecessary, and omitting this step reduces the number of hyperparameters. Pruning parameters is effectively equivalent to training them to zero.

Algorithm 2: Dimension Selection Algorithm of SDT-P

Input: A small subset of Dataset \mathcal{D} , warmup epochs E , number of layers L , total channels D , total states H , state sparsity β_0 , channel sparsity α_0 , state update fraction β , channel update fraction α

```

/* Warmup Epochs */  

Perform full update on SSM modules using  $\mathcal{D}$  for  $E$  epochs;  

/* Categorize Dimensions */  

for  $l = 1$  to  $L$  do  

  /* Set dimensions as zero */  

  Sort channels based on  $\|\bar{\mathbf{A}}^{(d)}\|$ ;  

  Select final  $(1 - \beta_0)D$  channels as zero channels and denote non-zero channels as set  $\mathbb{D}$ ;  

  for  $d \in \mathbb{D}$  do  

    Sort states based on magnitude of  $\bar{\mathbf{A}}_h^{(d)}$  at each state dimension;  

    Select final  $(1 - \alpha_0)H$  states as zero states and denote non-zero states as set  $\mathbb{H}$ ;  

  /* Unfreeze dimensions */  

  Sort non-zero channels  $\mathbb{D}$  based on changes of  $\|\bar{\mathbf{A}}^{(d)}\|$ ;  

  Select the top  $\beta\mathbb{D}$  channels as updatable, denoted by  $\mathbb{D}'$ ;  

  for  $d \in \mathbb{D}'$  do  

    Sort non-zero state dimensions based on changes of  $\|\bar{\mathbf{A}}^{(d)}\|$ ;  

    Select the top  $\alpha\mathbb{H}$  states as updatable at the  $d$ -th channel;

```

D.3 Details of Sec. 5.3: Expressive Power of SDT-P Combined with LoRA**D.3.1 Extending the Analysis to Deep S4 Models**

Our previous analysis in Sec. D.1 focused on single-channel S4 models. We now expand our investigation to more complex scenarios involving deep S4 models for both target and frozen architectures, incorporating D channels and varying layer depths. In this section, in addition to SDT-P, we introduce SDT+. The key difference between SDT+ and SDT-P is that SDT-P operates only on the SSM module, while SDT+ extends it to linear projection matrices. SDT+ exclusively updates the columns of weight matrices corresponding to the updatable channels identified through Alg. 2. In contrast, SDT-P operates only on SSM module and requires LoRA to modify the linear projection matrices. Notably, the linear projection matrix updates in SDT+ are inherently low-rank, making it a special case of SDT-P combined with LoRA. Our analysis begins with SDT+, which naturally extends to SDT-P with LoRA.

In this analysis, we assume that each input token x_t belongs to \mathcal{X} , a bounded subset of \mathbb{R}^D , and that the length of the input sequence is finite. Let the frozen model have L layers, and the target model have L^* layers, where $L > L^*$. Similar to the technique used in [Zeng & Lee \(2024\)](#) and [Giannou et al. \(2023\)](#). The basic idea of updating the frozen model to match the functionality of the target model is to utilize every $\lceil L/L^* \rceil$ layers of the frozen model to approximate every layer of the target model. We start introducing this proof idea from the simplest case where $L^* = 1, L = D$. In this scenario, we can simply choose one different channel to tune and maintain all other channels at zero at every layer. The outputs from the various channels of the deep S4 layers are then combined through a residual connection. This proof idea inspires us to perform channel selection and make use of the residual connections, which is the first and third step of SDT-P presented in Sec. 5. Building on this idea, we present the following results for when the target model has only $L^* = 1$ layer, and $L = D = 2$.

Lemma 7. *Consider a D -dimensional input sequence. Assume that the linear layers in the model have linear activation functions. Using SDT+, any deep S4 model with H hidden states per channel and L layers can be updated to accurately present any target one-layer deep S4 model without residual connections, having a reduced hidden state dimension $H^* < H$. Then this can be achieved by selectively fine-tuning at most $\lceil D/L \rceil$ channels, H^* hidden states, and residual connections at each layer, while additionally fully fine-tuning the linear projection matrix of the last layer only.*

Proof of Lemma 7. In this proof, we start by considering the case where $L = D$. In this case, we update a single distinct channel for each layer while setting the other channels to zero. Essentially, we modify the frozen model so that each layer corresponds to and functions as an individual channel in the target model. To be more specific, we fully update the first channel in the first layer to match the first channel of the target model, second channel in the second layer to match the second channel of the target model, so on and so forth.

For the l -th layer of the frozen model, we append subscript l to all parameters of the deep S4 layer as introduced in equation 4. For the d -th channel, corresponding notations are denoted with a superscript (d) . We define the t -th intermediate output token of the l -th deep S4 layer as $\mathbf{z}_{l,t} \in \mathbb{R}^D$. Additionally, the updated S4 module in layer l is denoted as $\widehat{\text{S4}}_l$, with $\widehat{\text{S4}}_{l,t}$ referring specifically to the sub-function that outputs the t -th token. Therefore, for the t -th intermediate output token of the l -th deep S4 layer of the updated model can be written as

$$\begin{aligned}\mathbf{z}_{l,t} &= \widehat{\mathbf{W}}_l \cdot \widehat{\text{S4}}_{l,t}(\mathbf{z}_{l-1,1}, \dots, \mathbf{z}_{l-1,t}) + \widehat{\beta}_l + \widehat{\mathbf{u}}_l \otimes \mathbf{z}_{l-1,t} \\ &= \widehat{\mathbf{W}}_l \cdot \begin{bmatrix} \widehat{\text{S4}}_{l,t}^{(1)}(\mathbf{z}_{l-1,1}^{(1)}, \dots, \mathbf{z}_{l-1,t}^{(1)}) \\ \vdots \\ \widehat{\text{S4}}_{l,t}^{(D)}(\mathbf{z}_{l-1,1}^{(D)}, \dots, \mathbf{z}_{l-1,t}^{(D)}) \end{bmatrix} + \widehat{\beta}_l + \widehat{\mathbf{u}}_l \otimes \mathbf{z}_{l-1,t},\end{aligned}$$

where $\widehat{\mathbf{W}}_l \in \mathbb{R}^{D \times D}$, $\widehat{\beta}_l \in \mathbb{R}^D$ are the updated weight and biases of the l -th layer of the frozen model, and $\widehat{\mathbf{u}}_l \in \mathbb{R}^D$ is the updated residual connection weight of the frozen model.

For layers $l < L = D$. We follow the steps provided in Sec. 5 to update the l -th layer of the frozen model such that it functionally equivalent to the l -th channel of the target model. For the reader's convinence, we restate our strategies here:

- **(Channel Selection)** Select $D' \leq D$ ($D' = 1$ here) important channels for making predictions. Any channel d that is not utilized will have their corresponding $\mathbf{C}^{(d)}$ set to zero, eliminating the need to update parameters for $\mathbf{A}^{(d)}$ and the d -th column of \mathbf{W} . To be more specific, we let $\mathbf{C}^{(d)} = \mathbf{0}$ for all $d \neq l$ in this scenario.
- **(Hidden State Selection)** Within the selected channels, select $H' \leq H$ important hidden states. For any hidden state that is not used within a selected channel d , the corresponding element in $\mathbf{C}^{(d)}$ will be set to zero, thus eliminating the need to tune the corresponding element in $\mathbf{A}^{(d)}$. To be more specific, we can achieve $\widehat{\text{S4}}_{l,t}^{(l)}(\cdot) = \text{S4}_{\star,t}^{(l)}(\cdot)$ by Lemma 2.
- **(Residual and Bias Tuning)** Regardless of other selections, SDT consistently tunes the coefficients of residual connections and biases in linear projections, as these components contain a negligible number of parameters. In this scenario, we let $\widehat{\beta}_l = \mathbf{0}$, $\widehat{\mathbf{u}}_l = [\underbrace{1 \dots 1}_{l-1 \text{ elements}} \ 0 \ \underbrace{1 \dots 1}_{D-l \text{ elements}}]^\top$.

This construction yields

$$\mathbf{z}_{l,t} = \begin{bmatrix} \mathbf{z}_{l-1,t}^{(1)} & \dots & \mathbf{z}_{l-1,t}^{(l-1)} & \text{S4}_{\star,t}^{(l)}(\mathbf{z}_{l,1}^{(l)}, \dots, \mathbf{z}_{l,t}^{(l)}) & \mathbf{z}_{l-1,t}^{(l+1)} & \dots & \mathbf{z}_{l-1,t}^{(D)} \end{bmatrix}^\top.$$

Consequently, only the l -th channel is active in the l -th layer, while all other layers function as identity mappings, propagating the output of the preceding layer without modification.

For layer $l = L = D$. Based on the setup of the first $L - 1$ layers, we have

$$\mathbf{z}_{L-1,t} = \begin{bmatrix} \text{S4}_{\star,t}^{(1)}(\mathbf{x}^{(1)}) & \dots & \text{S4}_{\star,t}^{(L-1)}(\mathbf{x}^{(L-1)}) & \mathbf{x}^{(L)} \end{bmatrix}^\top.$$

For the last layer, we let

$$\begin{aligned}\widehat{\mathbf{W}}_L &= \mathbf{W}_\star, \quad \widehat{\beta}_L = \beta_\star, \quad \widehat{\mathbf{u}}_L = \mathbf{0}, \\ \widehat{\text{S4}}_{L,t}^{(L)}(\cdot) &= \text{S4}_{\star,t}^{(L)}(\cdot), \text{ which can be achieved by Lemma 2.}\end{aligned}$$

It is easy to verify that the output of the updated frozen model is identical to the output of the target model, i.e.,

$$\mathbf{y}_t = \mathbf{z}_{L,t} = \mathbf{W}_* \begin{bmatrix} \text{S4}_{*,t}^{(1)}(\mathbf{x}^{(1)}) & \dots & \text{S4}_{*,t}^{(L-1)}(\mathbf{x}^{(L-1)}) & \text{S4}_{*,t}^{(L)}(\mathbf{x}^{(L)}) \end{bmatrix}^\top + \boldsymbol{\beta}_*.$$

Thus far, we have demonstrated that the statement holds when $L = D$. This analysis can be readily extended to cases where $L \neq D$ by tuning $\lceil D/L \rceil$ channels at each layer. For example, when $L = D/2$, we can tune two channels per layer using a construction similar to the one described above. This generalization completes the proof. \square

Theorem 2 (Expressive Power of SDT+ on Deep S4 Models). *Consider a D -dimensional input sequence. Assume that the linear layers in the model have linear activation functions. Using SDT+, any deep S4 model with H hidden states per channel and L layers can be updated to accurately present any target deep S4 model without residual connections, having a reduced hidden state dimension $H^* < H$, and fewer layers $L^* < L$. This can be achieved by selectively fine-tuning at most $\lceil DL^*/L \rceil$ channels, H^* hidden states, and residual connections at each layer.*

Proof of Theorem 2. We update every $\lceil D/L \rceil$ layers of the frozen model to approximate each layer of the target model. By applying Lemma 7 iteratively to each set of $\lceil D/L \rceil$ layers, we obtain the desired result. \square

Theorem 2 leads to the following result, which represents the deep S4 model case of Theorem 1.

Theorem 3 (Expressive Power of SDT-P on Deep S4 Models). *Consider a D -dimensional input sequence. Assume that the linear layers in the model have linear activation functions. By applying SDT-P to the S4 module and LoRA to the linear projection matrices, any deep S4 model with H hidden states per channel and L layers can be updated to accurately present any target deep S4 model without residual connections, having a reduced hidden state dimension $H^* < H$, and fewer layers $L^* < L$. This can be achieved by selectively fine-tuning at most $\lceil DL^*/L \rceil$ channels, H^* hidden states on SSM modules, applying rank- $\lceil \frac{L}{L^*} \rceil$ updates on linear projection matrices and updating residual connections and biases at each layer, while additionally fully fine-tuning the linear projection matrix of the last layer only.*

Proof of Theorem 1. Since SDT+ is a special case of SDT-P combined with LoRA, Theorem 2 directly implies the desired statement. \square

D.3.2 Extending the Analysis to S6

In this section, we extend the discussion of SDT-P combined with LoRA and SDT+ to S6, following the same logic. We begin by proving results for SDT+ in the scenario where the target model consists of only a single layer. In doing so, we extend Theorem 3 to apply to deep S6 models by first generalizing Lemma 7 to Lemma 8.

Lemma 8. *Consider a D -dimensional input sequence. Assume that the linear layers in the model have linear activation functions. Using SDT+, any deep S6 model with H hidden states per channel and L layers can be updated to accurately present any target one-layer deep S6 model without residual connections, having a reduced hidden state dimension $H^* < H$. Then this can be achieved by selectively fine-tuning at most $\lceil D/L \rceil$ channels, H^* hidden states, and residual connections at each layer, while additionally fully fine-tuning the linear projection matrix of the last layer only.*

Proof of Lemma 8. To prove this, we can just follow exactly the same proof logic of proof of Lemma 7 and the t -th intermediate output token of the l -th deep S6 layer of the updated model can be similarly written as

$$\begin{aligned} \mathbf{z}_{l,t} &= \widehat{\mathbf{W}}_l \cdot \widehat{\text{S6}}_{l,t}(\mathbf{z}_{l-1,1}, \dots, \mathbf{z}_{l-1,t}) + \widehat{\boldsymbol{\beta}}_l + \widehat{\mathbf{u}}_l \otimes \mathbf{z}_{l-1,t} \\ &= \widehat{\mathbf{W}}_l \cdot \begin{bmatrix} \widehat{\text{S6}}_{l,t}^{(1)}(\mathbf{z}_{l-1,1}^{(1)}, \dots, \mathbf{z}_{l-1,t}^{(1)}) \\ \vdots \\ \widehat{\text{S6}}_{l,t}^{(D)}(\mathbf{z}_{l-1,1}^{(D)}, \dots, \mathbf{z}_{l-1,t}^{(D)}) \end{bmatrix} + \widehat{\boldsymbol{\beta}}_l + \widehat{\mathbf{u}}_l \otimes \mathbf{z}_{l-1,t}, \end{aligned}$$

where $\widehat{\mathbf{W}}_l \in \mathbb{R}^{D \times D}$, $\widehat{\boldsymbol{\beta}}_l \in \mathbb{R}^D$ are the updated weight and biases of the l -th layer of the frozen model, and $\widehat{\mathbf{u}}_l \in \mathbb{R}^D$ is the updated residual connection weight of the frozen model.

For layers $l < L = D$. We follow the steps provided in Sec. 5 to update the l -th layer of the frozen model such that it functionally equivalent to the l -th channel of the target model. For the reader's convinence, we restate our strategies here:

- **(Channel Selection)** Select $D' \leq D$ ($D' = 1$ here) important channels for making predictions. For any channel d that is not utilized, instead of directly setting the corresponding $\mathbf{C}^{(d)}$ to zero as in the deep S4 model, we set $\boldsymbol{\beta}_{\Delta}^{(d)}$ to be sufficiently large. According to the computation of SSM parameters described in equation 12, this ensures that $\overline{\mathbf{B}}_n^{(d)}$ is set to zero for all $d \neq l$ in this scenario. This approach is equivalent to setting $\mathbf{C}^{(d)}$ to zero, as both result in the channel producing all zeros.
- **(Hidden State Selection)** Within the selected channels, select $H' \leq H$ important hidden states. For any hidden state that is not used within a selected channel d , the corresponding entries in $\mathbf{A}^{(d)}$ will be set to sufficiently small. To be more specific, we can achieve $\widehat{\text{S6}}_{l,t}^{(l)}(\cdot) = \text{S6}_{\star,t}^{(l)}(\cdot)$ by Lemma 2, with $\overline{\mathbf{A}}$, $\overline{\mathbf{B}}$, and \mathbf{C} are now computed via equation 12.
- **(Residual and Bias Tuning)** Regardless of other selections, SDT+ consistently tunes the coefficients of residual connections and biases in linear projections, as these components contain a negligible number of parameters. In this scenario, we let $\widehat{\boldsymbol{\beta}}_l = \mathbf{0}$, $\widehat{\mathbf{u}}_l = [\underbrace{1 \cdots 1}_{l-1 \text{ elements}} \ 0 \ \underbrace{1 \cdots 1}_{D-l \text{ elements}}]^\top$.

This construction yields

$$\mathbf{z}_{l,t} = \begin{bmatrix} z_{l-1,t}^{(1)} & \dots & z_{l-1,t}^{(l-1)} & \text{S4}_{\star,t}^{(l)}(z_{l,1}^{(l)}, \dots, z_{l,t}^{(l)}) & z_{l-1,t}^{(l+1)} & \dots & z_{l-1,t}^{(D)} \end{bmatrix}^\top.$$

For the remaining layers, following the same steps leads to the desired results. \square

Following similar steps as in Sec. D.3.1, we derive the following two results.

Theorem 4 (Expressive Power of SDT+ on Deep S6 Models). *Consider a D -dimensional input sequence. Assume that the linear layers in the model have linear activation functions. Using SDT+, any deep S6 model with H hidden states per channel and L layers can be updated to accurately present any target deep S6 model without residual connections, having a reduced hidden state dimension $H^* < H$, and fewer layers $L^* < L$. This can be achieved by selectively fine-tuning at most $\lceil DL^* / L \rceil$ channels, H^* hidden states, and residual connections at each layer.*

Theorem 5 (Expressive Power of SDT-P on Deep S6 Models). *Consider a D -dimensional input sequence. Assume that the linear layers in the model have linear activation functions. Using SDT-P on S6 and LoRA on linear projection matrices, any deep S6 model with H hidden states per channel and L layers can be updated to accurately present any target deep S6 model without residual connections, having a reduced hidden state dimension $H^* < H$, and fewer layers $L^* < L$. This can be achieved by selectively fine-tuning at most $\lceil DL^* / L \rceil$ channels, H^* hidden states on SSM modules, applying rank- $\lceil \frac{L}{L^*} \rceil$ updates on linear projection matrices and updating residual connections and biases at each layer, while additionally fully fine-tuning the linear projection matrix of the last layer only.*

Combining Theorem 3 and 5 leads to Theorem 1.

D.4 Details of Sec. 5.4: Sparse Dimension Tuning

In this part, we provide the details of our experiments on overhead analysis. To assess the memory usage and runtime of SDT and LoRA, we conducted experiments on four different models, including both SSM and hybrid architectures. Unless specified otherwise, for each model and method, a dataset was generated with 2,500 batches of data samples, each batch comprising a random sequence of 1,500 tokens. The simulation was repeated four times, including dataset generation. All experiments were carried out on a single H100 GPU, and the reported metrics represent averages across the four simulations. Consistent with our previous experiments, we used the original hyperparameter settings, ensuring that SDT includes similar trainable parameters than LoRA.

Memory Usage Analysis The memory usage of LoRA and SDT is presented in Table 15. Our observations indicate that SDT requires less memory than LoRA. This difference can be attributed to the design of the LoRA adapters, which involve matrix multiplication of two low-rank matrices. In contrast, tuning SSM with the same number of parameters does not require any matrix multiplication, resulting in lower memory usage.

| Memory Usage (GB) | Mamba-I-130M | Mamba-I-1.4B | Jamba-Tiny-319M | Jamba-Mini-52B |
|-------------------|--------------|---------------|-----------------|----------------|
| LoRA | 7.753 | 37.167 | 7.207 | 71.986 |
| LoRA & SDT | 5.738 | 26.491 | 6.605 | 67.193 |

Table 15: Memory usage comparison between SDT and LoRA on various models. **Bold** numbers indicate the lowest memory usage for each model.

Runtime Analysis Fine-tuning with SDT consists of two stages: (1) dimension selection and (2) standard training. In this study, we first compare the runtime of SDT and LoRA during stage 2 (training) and then evaluate the additional runtime introduced by SDT during stage 1 (dimension selection). Our results show that the dimension selection stage adds only marginal runtime overhead, and SDT is more efficient than LoRA in standard training.

Training: When the channels and states have been selected, the training of SDT is faster than LoRA when the same number of trainable parameters are considered.

The runtimes are reported in Table 16. We observe that, despite having more trainable parameters, SDT is faster than LoRA. We attribute this to the fact that LoRA introduces additional FLOPs due to the extra matrix multiplication operations required for each update (specifically, the multiplication of two low-rank matrices).

| Avg. Runtime (Seconds) | Mamba-I-130M | Mamba-I-1.4B | Jamba-Tiny-319M | Jamba-Mini-52B |
|------------------------|------------------|-------------------------------------|------------------------------------|--------------------------------------|
| LoRA | 410.0 ± 80.0 | 2060.0 ± 135.0 | 352.5 ± 107.5 | 3427.5 ± 185.0 |
| LoRA & SDT | 330.0 ± 77.5 | 1697.5 ± 87.5 | 257.5 ± 72.5 | 3065.0 ± 232.5 |

Table 16: Runtime comparison of SDT and LoRA during stage 2 (training).

Dimension Selection: For dimension selection, our method first performs an Initial Subset Training, and then selects the dimensions based on the magnitude of parameter changes across different dimensions.

1. *Initial Subset Training:* We update the model by going through only a subset of the dataset (e.g., 3% of batches in DART experiments), which is sufficient in practice.
2. *Magnitude-Based Dimension Selection:* After the subset training, we select dimensions based on the magnitude of parameter changes observed.

In this experiment, we simulate a real scenario using datasets with 2,500 batches, considering a small subset containing 125 batches (5% of the full dataset). We repeat the experiments 80 times, and the reported numbers are averaged across these simulations. The following table presents the runtime analysis of the dimension selection stage in SDT.

Table 17 demonstrates that the dimension selection stage adds only negligible runtime.

| Avg. Runtime (Seconds) | Mamba-I-130M | Mamba-I-1.4B | Jamba-Tiny-319M | Jamba-Mini-52B |
|-------------------------------------|----------------------------------|----------------------------------|----------------------------------|----------------------------------|
| Initial Subset Training | 16.250 ± 3.880 | 85.250 ± 5.130 | 15.750 ± 1.000 | 163.630 ± 10.120 |
| Magnitude-Based Dimension Selection | 0.280 ± 0.000 | 0.520 ± 0.120 | 0.090 ± 0.000 | 0.240 ± 0.040 |
| Total Time | 16.530 ± 3.880 | 85.770 ± 5.250 | 15.840 ± 1.000 | 163.870 ± 10.160 |
| Proportion of Training 1 Epoch | $0.050 \times$ | $0.051 \times$ | $0.062 \times$ | $0.053 \times$ |
| Proportion of Training 5 Epoch | $0.010 \times$ | $0.010 \times$ | $0.012 \times$ | $0.011 \times$ |

Table 17: Runtime comparison of SDT and LoRA during stage 1 (dimension selection).

| Method | # Params (%) | Accuracy |
|------------------------|--------------|-------------|
| Frozen | 0.00 | 73.9 |
| LoRA (Proj) | 16.00 | 77.6 |
| LoRA (S4+Proj) | 15.52 | 77.6 |
| LoRA (Proj) & SDT (S4) | 11.17 | 78.0 |
| Full Fine-Tuning | 100.00 | 77.6 |

Table 18: Accuracy comparison between SDT and LoRA on deep S4 models for CIFAR-10 (Krizhevsky et al., 2009).

E Expanded Sec. 6: Evaluation of SDT

E.1 Experiments on Deep S4 Models

Synthetic. For selecting channels and hidden states, we initiate with a warmup learning rate between $1e - 2$ and $1e - 3$ and conduct 20 warmup iterations. Learning rates are adjusted between $5e - 2$, $1e - 2$, $5e - 3$, and $1e - 3$. We apply LoRA with ranks of 2 and 4 to the SSM and with ranks of 4, 8, and 16 to the linear projection matrices. Non-zero states are selected from the sets $\{4, 8\}$, and non-zero channels from $\{8, 16\}$.

CIFAR-10 (Krizhevsky et al., 2009). Previous work (Dinh et al., 2022) demonstrates that large language models can be fine-tuned for image classification tasks. Here, we consider the this challenging task of adapting SSMs for computer vision. In this experiment, we conduct experiments on the CIFAR-10 dataset (Krizhevsky et al., 2009). We employ an eight-layer deep S4 model with a hidden state dimension of 16 and a model dimension of 64. Since pretrained deep S4 models are not available, we simulate a pretrained scenario by fully updating the model for 50 epochs first, then subsequently evaluating the PEFT methods over an additional 5 epochs. We adhere to the preprocessing steps for CIFAR-10 as outlined by Gu et al. (2022a). The LoRA ranks for linear projection matrices are tuned among $\{1, 2, 4, 8, 16\}$, and for the S4 component, ranks are set from $\{1, 2, 4\}$. Non-zero states are chosen from $\{8, 12, 16\}$, and non-zero channels from $\{48, 64\}$. A warmup phase includes 1 epoch with a learning rate of $1e - 2$. For linear projection matrices, LoRA ranks are explored at $\{2, 4, 8, 16\}$, and for the SSM, ranks at $\{2, 4, 8\}$. All state dimensions are updated, and channel dimensions considered for updates are $\{4, 8, 16, 32\}$. The results, as reported in Table 18, indicate that SDT outperforms LoRA with fewer trainable parameters.

E.2 Experiments on Mamba-I, Mamba-II, and Jamba

Here, we provide more experiment details. Unless otherwise stated, our experiment setting is identical to Sec. C.1. For LoRA, we consider three different LoRA configurations at each layer, involving the following matrices which comprise most of the parameters: \mathbf{W}_{out} (output linear projection), \mathbf{W}_B , \mathbf{W}_C (weight matrices for computing input-dependent \mathbf{B}_n , \mathbf{C}_n), and $\mathbf{W}_{\Delta,\downarrow}$, $\mathbf{W}_{\Delta,\uparrow}$ (down and up projection matrices of LoRA adapters for computing Δ). The three LoRA application methods are: (i) \mathbf{W}_{out} , \mathbf{W}_B , \mathbf{W}_C , and $\mathbf{W}_{\Delta,\downarrow}$, $\mathbf{W}_{\Delta,\uparrow}$; (ii) \mathbf{W}_{out} , \mathbf{W}_B , \mathbf{W}_C and $\mathbf{W}_{\Delta,\downarrow}$; and (iii) \mathbf{W}_{out} and $\mathbf{W}_{\Delta,\uparrow}$. For SDT, we set the channel freeze ratio at 99% across all scenarios. We select the state freeze ratio α from the set $\{75\%, 90\%, 95\%\}$ and apply LoRA exclusively to \mathbf{W}_{out} to maintain a comparable number of trainable parameters. Residual connections and bias are frozen in this experiment. For the warmup, we employ 500 data batches to fully train the SSM modules prior to dimension selection, except for the RTE task in GLUE, where we use 250 batches due to its limited dataset size. Note that the parameters are reverted back after the warmup stage.

Additional Results on Mamba-II. For Mamba-II, applying SDT is not straightforward because Mamba-II further constrains A such that all (non-zero) entries must have the same value. Therefore, our original dimension selection approach cannot be directly applied here. We consider a naive extension of SDT by selecting dimensions in the projection matrices for input mapping vector B and the projection matrices for output mapping vector C using their respective magnitude, and fine-tune the selected dimensions and all elements of state transition matrix A .

Tables 19 and 20 compare the performance on Mamba-II. The results demonstrate that SDT consistently outperforms LoRA on Mamba-II models.

| Model | Mamba-II-130M | | | | Mamba-II-1.3B | | | |
|------------|-------------------------------|------------|--------------|--------------|---------------|--------------|--------------|--------------|
| | Dataset Metric (\uparrow) | Params (%) | DART | | Params (%) | SAMSum | | Spider Acc. |
| | | | METEOR | BLEU | | R1 | R2 | |
| LoRA | 0.3354 | | 68.71 | 48.09 | 0.1614 | 49.73 | 26.14 | 41.53 |
| LoRA & SDT | 0.3393 | | 70.60 | 48.93 | 0.1767 | 50.72 | 27.21 | 42.54 |

Table 19: Performance comparison between SDT and LoRA on Mamba-II-130M and Mamba-II-1.3B. **Bold** numbers indicate the best performance for each task.

| Model | Mamba-II-130M | | | | | | |
|------------|---------------------------------|------------|-------------|-------------|-------------|-------------|-------------|
| | Dataset Accuracy (\uparrow) | Params (%) | GLUE | | | | Spider Acc. |
| | | | RTE | MRPC | SST2 | QNLI | |
| LoRA | 0.3354 | | 63.4 | 80.9 | 89.1 | 85.3 | 87.1 |
| LoRA & SDT | 0.3393 | | 64.3 | 82.3 | 94.1 | 87.0 | 88.3 |

Table 20: Performance comparison between SDT and LoRA on GLUE (Wang et al., 2019) dataset using Mamba-II-130M. **Bold** numbers indicate the best performance for each task.

Additional Results on Jamba. Table 21 shows results for SDT and LoRA on additional datasets. Even though the performance improvement is smaller, our method outperforms pure LoRA in most cases. Mamba layers make up only a small part of Jamba, which is a possible reason for smaller performance gains.

| LinProj | S6 | GLUE Avg. | DART | | CelebA Acc. | SAMSum | | | Spider Acc. |
|---------|------|-------------|-------------|-------------|-------------|-------------|-------------|-------------|-------------|
| | | | BLEU | MET. | | R1 | R2 | RL | |
| LoRA | LoRA | 65.5 | 52.9 | 73.0 | 88.5 | 56.4 | 33.5 | 47.9 | 90.7 |
| | SDT | 67.7 | 53.1 | 73.0 | 88.4 | 56.5 | 33.5 | 48.0 | 89.8 |

Table 21: **Performance comparison between SDT and LoRA on pretrained Jamba models.** **Bold** numbers indicate the best performance for each task. We use Jamba-Tiny-319M to compare the performance of SDT and LoRA on GLUE (Wang et al., 2019), and CelebA (Liu et al., 2015) benchmarks. For all other datasets, we employ Jamba-Mini-52B. We report only the best setting out of three for each method.

Additional Results for LoRA+. We have included evaluations of LoRA+ (Hayou et al., 2024) (an advanced LoRA variant) alongside LoRA+ with SDT to provide a more comprehensive analysis. We extended our investigation to include LoRA+ with SDT and evaluated its performance against LoRA+ across various datasets on both Mamba-I and Mamba-II. The results, presented in Table 22, show that integrating SDT with LoRA+ enhances its effectiveness and achieves superior performance compared to using LoRA+ alone.

| Model | Mamba-I-130M | | Mamba-II-130M | | Mamba-II-1.3B | | | |
|-------------------------------|--------------|--------------|---------------|--------------|---------------|--------------|-------------|--------------|
| | DART | | DART | | SAMSum | Spider | | |
| Dataset Metric (\uparrow) | METEOR | BLEU | METEOR | BLEU | R1 | R2 | RL | Acc. |
| LoRA+ | 70.06 | 50.91 | 69.78 | 49.14 | 49.83 | 26.09 | 41.66 | 73.75 |
| LoRA+ & SDT | 70.58 | 51.93 | 70.48 | 49.99 | 50.81 | 27.19 | 42.4 | 84.22 |

Table 22: Performance comparison between LoRA+ and SDT on Mamba-I and Mamba-II. **Bold** numbers indicate the best performance for each task. We test all experiments under various parameter settings ($<0.4\%$) for both LoRA+ and SDT, and report the best values.